Available online at www.sciencedirect.com
ScienceDirect
Physica D 237 (2008) 755–773
PHYSICA D
www.elsevier.com/locate/physd

Additive noise-induced Turing transitions in spatial systems with application to neural fields and the Swift–Hohenberg equation

Axel Hutt[a,*], Andre Longtin[a], Lutz Schimansky-Geier[b]

[a] *Department of Physics, 150 Louis Pasteur, University of Ottawa, Canada*
[b] *Humboldt University at Berlin, Institute of Physics, Newtonstr. 15, 12489 Berlin, Germany*

Received 30 May 2007; received in revised form 11 October 2007; accepted 22 October 2007
Available online 28 October 2007

Communicated by S. Coombes

Abstract

This work studies the spatio-temporal dynamics of a generic integral–differential equation subject to additive random fluctuations. It introduces a combination of the stochastic center manifold approach for stochastic differential equations and the adiabatic elimination for Fokker–Planck equations, and studies analytically the systems' stability near Turing bifurcations. In addition two types of fluctuation are studied, namely fluctuations uncorrelated in space and time, and global fluctuations, which are constant in space but uncorrelated in time. We show that the global fluctuations shift the Turing bifurcation threshold. This shift is proportional to the fluctuation variance. Applications to a neural field equation and the Swift–Hohenberg equation reveal the shift of the bifurcation to larger control parameters, which represents a stabilization of the system. All analytical results are confirmed by numerical simulations of the occurring mode equations and the full stochastic integral–differential equation. To gain some insight into experimental manifestations, the sum of uncorrelated and global additive fluctuations is studied numerically and the analytical results on global fluctuations are confirmed qualitatively.

Keywords: Stochastic center manifold; Adiabatic elimination; Spatially colored noise; Integral–differential equation

1. Introduction

The dynamics in spatially extended systems have attracted much attention in recent decades [1–3]. In this context, the study of macroscopic changes, i.e. phase transitions, of the system plays an important role. For example the successful explanation of visual hallucinations in humans by a phase transition in neuronal populations [4,5] supported the idea of nonlocal interactions in neural systems [6–12]. Although the notion of a phase transition is defined rigorously in thermodynamical equilibrium only, the mathematical description of transitions in systems far from equilibrium has been very successful [13,14]. On a descriptive level, phase transitions in the thermodynamical equilibrium and far from it reflect a persistent change of macroscopic spatio-temporal dynamics while changing a few so-called control parameters.

Since natural systems exhibit internal and external random fluctuations, the mathematical description of non-equilibrium phase transitions should take them into account. The corresponding theory is well-developed [15–19] and has been applied successfully to phase transitions in general low-dimensional systems [20–25], in spatial physical systems [26–31], and in biological systems [32–36]. In this context, most studies on spatial systems examine the linear stability, and there are fewer that focus on the nonlinear effects in the presence of noise. Since the nonlinear stochastic analysis of spatially extended systems is mathematically very challenging, there are different methods to study systems assuming specific system properties [13,15,37,18,29,31,32,36–39]. For example, it is well known how to treat stochastic system, whose deterministic version obeys a potential dynamics; see e.g. [13,15,37]. Moreover, important stochastic adiabatic

* Corresponding author.
E-mail addresses: ahutt@uottawa.ca (A. Hutt), alongtin@uottawa.ca (A. Longtin), alsg@physik.hu-berlin.de (L. Schimansky-Geier).

0167-2789/$ - see front matter © 2007 Elsevier B.V. All rights reserved.
doi:10.1016/j.physd.2007.10.013

elimination procedures have been developed for systems whose deterministic part and noise strength share specific scalings; see e.g. [37].

The present work aims to treat a general class of spatial systems, namely stochastic integro-differential equations involving nonlocal spatial interactions, which in general do not fulfill the previous conditions. Hence our work was motivated by the general question of how to treat spatially extended systems with very few specific properties. Looking for methods, we concluded that the combination of a center manifold-like approach [24,29,40,41] and an adiabatic elimination procedure [42] is best suited to the analytical treatment of stochastic integral–differential equations. This choice appeared optimal with respect to the applicability of both methods to rather unspecified problems. To be more specific, the subsequent sections considers a stochastic center manifold approach [40,41], which has been applied in the work of Xu and Roberts [40] to a low-dimensional stochastic model in order to gain a single order parameter. These authors showed that the model does not reduce to a single order parameter equation immediately due to several occurring colored-noise fluctuations. To deal with these fluctuations, inter alia they applied successfully a Fokker–Planck approach which assumes the Gaussian-like shape of probability densities. Our work extends the latter study in several aspects. At first it applies the stochastic center manifold approach to spatially extended systems. Further, we remove the Gaussian assumption in [40] by applying an adiabatic elimination procedure for the Fokker–Planck equations [38,42]. This method applies an adiabatic procedure for spatially extended systems based on the corresponding Fokker–Planck equations. However, the power of this technique results from the knowledge of the appropriate scaling behavior of projection amplitudes which might not be known for general systems. In turn this knowledge might be gained for general systems by deterministic center manifold techniques. Consequently an optimal analysis consists in the first application of a deterministic center manifold technique to gain the appropriate scaling, followed by the stochastic center manifold approach leading to a reduced set of equations. Then the subsequent application of the adiabatic elimination procedure allows for the final extraction of the single order parameter equation. These extensions have been applied recently to the stochastic Swift–Hohenberg equation [43]. The present work applies the latter extensions to stochastic integral–differential equations and thus generalizes and extends the results obtained in [43].

The present work was also motivated by the question how to treat mathematically the effect of additive fluctuations near the stability threshold taking into account nonlinear terms. A first choice considers random fluctuations uncorrelated in space and time. Such fluctuations may originate from thermal background activity and have been measured experimentally in spatial systems [44,45]. Further, spatially correlated fluctuations have been shown to yield pattern formation for multiplicative [18, 46–48] and additive noise [49–52]. The present work studies global fluctuations, which are homogeneous in space and uncorrelated in time. Such fluctuations have attracted some attention in the last years and we mention experimental effects by periodic [50] and randomly dichotomous temporal fluctuations [51]. This specific choice of fluctuations allows for the analytical treatment of stochastic phase transitions in the nonlinear regime and we can show noise-induced effects for additive fluctuations.

Our work studies the Turing phase transition in a stochastic integral–differential equation (IDE) and considers the effects of uncorrelated and global fluctuations on general pattern forming systems with applications to neural field and the Swift–Hohenberg equation. Since the latter models have been studied extensively in recent decades, the model under discussion is supposed to represent a general model for nonlocal interactions. The IDE reads

$$\frac{\partial U(x,t)}{\partial t} = h[U(x,t)] + \int_{\Omega} \mathrm{d}y\, (K(x-y)S_K[U(y,t)] + L(x-y)S_L[U(y,t)]) + I(x,t). \tag{1}$$

in the one-dimensional spatial domain Ω. The activity $U(x,t)$ may be interpreted differently corresponding to the system under study. For example, in neural fields $U(x,t)$ represents the effective membrane potential of neural populations [53, 54], whereas in hydrodynamics Eq. (1) may be written as the Swift–Hohenberg equation [55], where $U(x,t)$ is a hydrodynamic amplitude. Further, the functional $h[U]$ represents the local dynamics, $S_K[U], S_L[U]$ reflect the (non)linear interaction functionals and $I(x,t)$ denotes an external spatio-temporal input. Moreover, $K(x)$ and $L(x)$ are spatial interaction kernels of two different types of interaction. One may interpret $K(x), L(x)$ as weighted probability density functions of spatial interactions between two spatial locations at distance x. For instance, $K(x) = \text{const}$ represents mean-field coupling while no spatial coupling is given by $K(x) = \delta(x)$. An additional important case is $K(x) > 0$ and $L(x) < 0$, which reflects excitatory and inhibitory interaction, respectively, and allows for various space–time phenomena [5,7,53,54,56–58]. In the following, we consider symmetric kernels with $K(x) = K(-x)$ and $L(x) = L(-x)$.

In addition, the different combinations of the local dynamics, the interaction functions and the spatial interactions yield diverse dynamical behavior. For instance nonlinear local dynamics, linear interactions and short-range spatial interactions represent a reaction–diffusion system [55], while a mixture of short-range/long-range kernels and linear/nonlinear interactions is present in the Kuramoto–Sivashinsky equation exhibiting spatio-temporal chaos [55]. We point out that these different models are specific cases of the model (1). In the following we pick two diverse prominent examples of pattern forming systems to illustrate the universality of the model and the approach.

This work is structured as follows:

- Section 2 introduces the transformation of the spatial system into the spatial Fourier space and shows the mathematical formulation for stochastic differential equations (SDEs) and the corresponding Fokker–Planck equation (FPE). Uncorrelated and global fluctuations are introduced and their effect on the SDEs and FPE is discussed.

- Section 3 studies the linear dynamics of the system for uncorrelated and global fluctuations and reveals the major differences between both fluctuation types.
- Section 4 introduces the stochastic center manifold approach for SDEs and the adiabatic elimination approach for the FPE. Further, it is shown how the combination of both methods yields a single order parameter equation for both fluctuation types. Moreover, we show that global fluctuations may shift the stability threshold of Turing bifurcations to larger values of the control parameter, i.e. to higher nonlinearity.
- Sections 5 and 6 show the application to a neural field equation and the Swift–Hohenberg equation, respectively. The analytical results from Section 4 are compared to numerical results from the reduced mode equations and the full integral–differential equation. Finally, Section 7 summarizes the results and provides an outlook on future work.

2. The Fourier picture

Most studies investigate phase transitions using few order parameters, which are assumed to reflect the most important properties of the dynamics. These include the study of statistical moments in space and the study of the structure function in Fourier space, namely the power spectrum of the spatial activity at each time point [17,18,27,28,59]. The present work studies the dynamics of the spatial system not in the spatial domain but in the corresponding Fourier space of the spatial domain. Thus our approach follows the idea of the structure function but examines the spatial Fourier modes separately in a system of equations. This approach has been proven to yield important results in the presence of additive stochastic fluctuations in several previous studies [29,60].

The evolution equation (1) may be written as the SDE

$$\mathrm{d}U(x,t) = f[U(x,t)]\mathrm{d}t + \mathrm{d}\Gamma(x,t), \tag{2}$$

with the drift term

$$f[U(x,t)] = h[U(x,t)] + \int_\Omega \mathrm{d}y\,(K(x-y)S_K[U(y,t)] + L(x-y)S_L[U(y,t)])$$

and the random fluctuations $\mathrm{d}\Gamma(x,t) = I(x,t)\mathrm{d}t$ at spatial location x. Here the random fluctuations are additive and thus represent external random stimuli which have been shown to reflect realistic inputs in biological systems, e.g. [61]. In principle the subsequent analysis steps also allow us to study random fluctuations of system parameters, which represents multiplicative noise and renders the analysis more complex. However, for illustration reasons the present work focusses on additive random fluctuations.

We assume periodic boundary conditions which discretize the Fourier space into infinitely many modes with the basis $\{\exp(-\mathrm{i}k_n x)/\sqrt{|\Omega|}\}$, $k_n = n2\pi/|\Omega|$ and the orthogonality condition

$$\frac{1}{|\Omega|}\int_\Omega \mathrm{e}^{\mathrm{i}(k_m-k_n)x}\mathrm{d}x = \delta_{nm}.$$

In the Fourier picture the activity variable $U(x,t)$ may be expanded by

$$U(x,t) = \frac{1}{\sqrt{|\Omega|}}\sum_{n=-\infty}^{\infty} u_n(t)\mathrm{e}^{\mathrm{i}k_n x} \tag{3}$$

with the corresponding Fourier projections $u_n(t) \in \mathcal{C}$ with $u_n = u^*_{-n}$. By virtue of the symmetry of spatial interaction kernels, i.e. $K(x) = K(-x)$, and the one-dimensionality of the spatial domain, the Fourier transform of the kernel functions is symmetric in spatial Fourier space. Hence the dynamics of the spatial modes $u_n(t)$ depend on k_n^2 and we find $u_n = u_{-n}$.

Then inserting the Fourier projection (3) into Eq. (2) yields the infinite set of SDEs

$$\mathrm{d}u_n(t) = \tilde{f}_n[\{u_j\}]\mathrm{d}t + \frac{1}{\sqrt{|\Omega|}}\int_\Omega \mathrm{d}x\,\mathrm{d}\Gamma(x,t)\mathrm{e}^{-\mathrm{i}k_n x} \tag{4}$$

with the Fourier transform $\tilde{f}_n[\cdot]$ of $f[\cdot]$. We observe that the evolution equation (2) is equivalent to the infinite set of evolution equations (4) in the Fourier space.

Now the random fluctuations $\mathrm{d}\Gamma(x,t)$ are assumed to represent a superposition of independent fluctuating sources with

$$\mathrm{d}\Gamma(x,t) = \int_\Omega \mathrm{d}y\, g(x,y)\,\mathrm{d}W(y,t). \tag{5}$$

The terms $\mathrm{d}W(y,t)$ represent the differentials of independent Wiener processes satisfying

$$\langle \mathrm{d}W(y,t)\rangle = 0,$$
$$\left\langle \mathrm{d}W(x,t)\mathrm{d}W(y,t')\right\rangle = 2\delta(x-y)\delta(t-t')\mathrm{d}t\mathrm{d}t'$$

where $\langle\cdot\rangle$ denotes the ensemble average and $g(x,y)$ is a weight kernel function. As will be seen in the subsequent paragraphs, g gives the spatial interaction of random fluctuations.

2.1. Spatially uncorrelated fluctuations

In the case of fluctuations uncorrelated in space and time, the fluctuations at each spatial location $\mathrm{d}\Gamma(x,t)$ are independent of the fluctuations at other locations. Hence the weight kernel function in (5) is $g(x,y) = \eta\delta(x-y)$ with the fluctuation strength η, and thus $\mathrm{d}\Gamma(x,t) = \eta\,\mathrm{d}W(x,t)$. Then Eq. (4) reads

$$\mathrm{d}u_n(t) = \tilde{f}_n[\{u_j\}]\mathrm{d}t + \eta\mathrm{d}W_n(t) \tag{6}$$

with

$$\mathrm{d}W_n(t) = \frac{1}{\sqrt{|\Omega|}}\int_\Omega \mathrm{d}x\,\mathrm{d}W(x,t)\mathrm{e}^{-\mathrm{i}k_n x}.$$

The terms $\mathrm{d}W_n(t)$ are the Fourier modes of the spatial Wiener processes $\mathrm{d}W(x,t)$ and represent Wiener processes themselves with

$$\langle \mathrm{d}W_n(t)\rangle = 0, \quad \left\langle \mathrm{d}W_n(t)\mathrm{d}W_l(t')\right\rangle = 2\delta_{nl}\delta(t-t')\mathrm{d}t\mathrm{d}t'.$$

In other words, fluctuations uncorrelated in space and time correspond to fluctuations uncorrelated in Fourier space and time.

The Fokker–Planck equation of Eq. (6) reads

$$\frac{\partial P(\{u_n\},t)}{\partial t} = -\sum_j \frac{\partial}{\partial u_j}\tilde{f}[\{u_n\}]P(\{u_n\},t) + \eta^2 \sum_j \frac{\partial^2}{\partial u_j^2} P(\{u_n\},t), \tag{7}$$

with the joint probability density $P(\{u_n\},t)$ of the stochastic process.

2.2. Spatially global fluctuations

In this case, the fluctuation source $\mathrm{d}\Gamma(x,t) = \mathrm{d}\Gamma(t)$ is constant in space, the weight kernel is given by $g(x,y) = \eta'\delta(y)$, and thus $\mathrm{d}\Gamma(x,t) = \eta'\,\mathrm{d}W(0,t) = \mathrm{d}W(t)$. In other words, at time t the random fluctuations are the same at each spatial location. Consequently Eq. (4) reads

$$\begin{aligned} \mathrm{d}u_n(t) &= \tilde{f}_n[\{u_j\}]\mathrm{d}t, \quad \forall n \neq 0 \\ \mathrm{d}u_0(t) &= \tilde{f}_0[\{u_j\}]\mathrm{d}t + \eta \mathrm{d}W(t) \end{aligned} \tag{8}$$

with $\eta = \eta'\sqrt{|\Omega|}$. Hence all spatial modes $u_{n\neq 0}(t)$ obey a deterministic ordinary differential equation and the dynamics of $u_0(t)$ is governed by an SDE subjected to the Wiener process $\mathrm{d}W(t)$.

In addition, the Fokker–Planck equation of (8) reads

$$\frac{\partial P(\{u_n\},t)}{\partial t} = -\sum_j \frac{\partial}{\partial u_j}\tilde{f}[\{u_n\}]P(\{u_n\},t) + \eta^2 \frac{\partial^2}{\partial u_0^2} P(\{u_n\},t). \tag{9}$$

In the subsequent section, we study the evolution equation (1) in the linear regime and examine its linear stability with respect to both uncorrelated and global fluctuations.

3. Linear stochastic analysis

Now let us study the activity about the stationary state U_0 constant in space and time. To this end we assume an external stimulation in (1) constant in space and time, i.e. $I(x,t) = I_0$. Then Eq. (1) recasts to the implicit equation for the stationary state

$$0 = h[U_0] + S_K[U_0]\int_\Omega K(x)\mathrm{d}x + S_L[U_0] \times \int_\Omega L(x)\mathrm{d}x + I_0. \tag{10}$$

Considering small deviations $z(x,t) = U(x,t) - U_0$ and random fluctuations $\xi(x,t) = I(x,t) - I_0 \ll I_0$, we find

$$\mathrm{d}z(x,t) = \left(h'\,z(x,t) + S_e' \int_\Omega K(x-y)z(y,t)\mathrm{d}y + S_i' \int_\Omega L(x-y)z(y,t)\mathrm{d}y\right)\mathrm{d}t + \mathrm{d}\Gamma(x,t) \tag{11}$$

with $\mathrm{d}\Gamma(x,t)$ taken from Eq. (5) and $h' = \delta h[U]/\delta U$, $S_e' = \delta S_K[U]/\delta U$ and $S_i' = \delta S_L[U]/\delta U$ computed at $U = U_0$. Here, and in the following, $\delta/\delta U$ denotes the functional derivative. Since Eq. (11) resembles Eq. (2), we can formulate the linear evolution equation (11) immediately in the Fourier picture according to the previous section.

3.1. Uncorrelated fluctuations

Applying the Fourier transformation to Eq. (11), we obtain from Eq. (6)

$$\mathrm{d}u_n(t) = \alpha_n\, u_n(t)\,\mathrm{d}t + \eta \mathrm{d}W_n(t) \tag{12}$$

with the Fourier transforms $u_n(t)$ of $z(x,t)$ and $\alpha_n = h' + \mathcal{F}[S_e'K(x) - S_i'L(x)](k_n)$ with

$$\mathcal{F}[f(x)](k) = \int_\Omega \mathrm{d}x f(x)\mathrm{e}^{-\mathrm{i}kx}. \tag{13}$$

In addition, we find the symmetry $\alpha_n = \alpha_{-n}$ due to the spatial symmetry of the kernels $K(x)$ and $L(x)$.

To study the stability of Eq. (12), first let us examine the deterministic case $\eta = 0$. We make the ansatz $u_n(t) \sim \exp(\lambda t)$, $\lambda \in \mathcal{C}$ and find $\lambda = \alpha_n$. Since the kernel functions and the functional $h[U]$ take real values, we find $\lambda \in \mathcal{R}$ and no oscillatory activity is present. Further, the system is linearly stable if $\alpha_n < 0$ for all n and it is marginally stable if some spatial modes satisfy $\alpha_n = 0$. When the global maximum of $\alpha_n = \alpha_n(k_n)$ becomes positive for some wavenumbers k_n, the system becomes unstable and shows a stationary phase transition. In this case the critical wavenumber reads [62]

$$k_c = \arg\max_{k_n} \mathcal{F}[K+L](k_c), \tag{14}$$

and for $k_c \neq 0$ the transition is called a Turing phase transition [63,64].

Adding random fluctuations, i.e. $\eta \neq 0$, we find the solution of (12) to be

$$u_n(t) = u_n(0)\,\mathrm{e}^{\alpha_n t} + \eta \int_0^t \mathrm{e}^{\alpha_n(t-t')}\mathrm{d}W_n(t')$$

with the initial value $u_n(0)$. This means that each spatial mode at wavenumber k_n is subjected to random fluctuations. It is easy to see that $\alpha_n < 0$ for all n guarantees bounded activity of each spatial mode, i.e. bounded activity of the system [24] for large times t. In other words the system is pathwise stable.

However, the random fluctuations $\mathrm{d}W_n(t)$ play an important role if the system approaches the stability threshold with $\alpha_n \to 0$ for a given n. To gain further information on the stationary stochastic process near the stability threshold, we examine the stationary joint probability density $P_s(\{u_j\})$ of (12) and obtain from (7) the well-known solution [37]

$$P_s(\{u_j\}) = \frac{1}{(\sqrt{2\pi}\,\eta)^N}\prod_{n=1}^N \sqrt{|\alpha_n|}\mathrm{e}^{-|\alpha_n|u_n^2/2\eta^2} \tag{15}$$

for $\alpha_n < 0$. This is the well-known multivariate Gaussian probability density with vanishing mean and covariance matrix $\boldsymbol{\sigma}$ with $\sigma_{nm} = \eta^2/|\alpha_n|\delta_{nm}$. In the absence of random fluctuations, i.e. $\eta \to 0$, we have $P_s \to \prod_n \delta(u_n)$, In addition,

just below the stability threshold some spatial modes u_c exhibit $\alpha_c \approx 0$, and the corresponding variance matrix element is very large. This phenomenon has been observed experimentally in many spatial systems, see e.g. [13,16], and the corresponding activity shows so-called critical fluctuations. In the case of $\alpha_n > 0$, where some modes are unstable, no stationary probability density exists.

3.2. Global fluctuations

In this case the Fourier expansion yields

$$\mathrm{d}u_n(t) = \alpha_n u_n(t)\mathrm{d}t + \eta\delta_{n,0}\mathrm{d}W(t)$$

with α_n taken from Eq. (12). In contrast to the case of uncorrelated fluctuations, now all spatial modes at wavenumbers $k_n \neq 0$ are deterministic and vanish for $\alpha_n < 0$ at large times, while the constant spatial mode with $k = 0$ fluctuates randomly subjected to $\mathrm{d}W(t)$. Similar to the treatment of uncorrelated fluctuations, $\alpha_n < 0$ for all n guarantees the pathwise stability of the system at each spatial location.

To gain further information on the stationary stochastic process near the stability threshold, we apply the results from the previous section and obtain from (9) the Fokker–Planck equation

$$\frac{\partial P(\{u_n\},t)}{\partial t} = -\sum_j \frac{\partial}{\partial u_j}\alpha_j P(\{u_n\},t) + \eta^2 \frac{\partial^2}{\partial u_0^2} P(\{u_n\},t).$$

The spatial modes $u_n(t)$ are independent of each other, and we find for $\alpha_n < 0$

$$P_s(\{u_j\}) = \frac{\sqrt{|\alpha_0|}}{\sqrt{2\pi}\,\eta} \mathrm{e}^{-|\alpha_0|u_0^2/2\eta^2} \prod_{n\neq 0}\delta(u_n). \tag{16}$$

Now critical fluctuations may occur if the spatial mode u_0 becomes pathwise unstable, i.e. $\alpha_0 \approx 0$. Similar to Section 3.1, no stationary probability density exists for $\alpha_n > 0$.

The latter analysis gives the stability criterion in the linear regime. When the system becomes linearly unstable, the system may still be stable for larger deviations from the stationary state if the nonlinearities bound the dynamics. In the subsequent section, this nonlinear saturation is studied in some detail for both uncorrelated and global fluctuations.

4. Nonlinear stochastic analysis

Now let us turn to the field activity in the nonlinear regime. The aim of this section is manifold:

- First, we formulate the nonlinear problem up to the cubic nonlinear order and give the evolution equation in the Fourier picture.
- Then we study the deterministic case to obtain the valid scaling orders for all occurring variables and constants.
- The subsequent subsection discusses the uncorrelated fluctuations at low expansion order and introduces the stochastic center manifold approach and the adiabatic elimination procedure for Fokker–Planck equations. This section shows in some detail the calculation procedure of both methods.
- Then both methods are applied in the case of global fluctuations at various expansion orders. We find analytically a shift of the bifurcation threshold by additive global fluctuations at high expansion order.

4.1. The nonlinear equation

Expanding the functionals $S_K[U]$ and $S_L[U]$ in (1) to cubic nonlinear order about the stationary point U_0 defined by Eq. (10), the evolution equation (1) reads

$$\mathrm{d}U(x,t) \approx \mathrm{d}\Gamma(x,t) + \left(\int_\Omega \mathrm{d}y\, K_1(x-y)U(y,t) + K_2(x-y)U^2(y,t) + K_3(x-y)U^3(y,t)\right)\mathrm{d}t \tag{17}$$

with

$$K_1(x) = \frac{\delta S_K}{\delta U}K(x) + \frac{\delta S_L}{\delta U}L(x) + \frac{\delta h}{\delta U}\delta(x)$$
$$K_2(x) = \frac{1}{2}\frac{\delta S_K^2}{\delta U^2}K(x) + \frac{1}{2}\frac{\delta^2 S_L}{\delta U^2}L(x) + \frac{1}{2}\frac{\delta^2 h}{\delta U^2}\delta(x)$$
$$K_3(x) = \frac{1}{6}\frac{\delta^3 S_K}{\delta U^3}K(x) + \frac{1}{6}\frac{\delta^3 S_L}{\delta U^3}L(x) + \frac{1}{6}\frac{\delta^3 h}{\delta U^3}\delta(x)$$

where the functional derivatives are computed at the stationary state $U = U_0$. Here we point out that the deterministic version of Eq. (17) generalizes several PDE-models, e.g. reaction–diffusion equations [55] such as the Ginsburg–Landau equation or the Newell–Whitehead equation, or PDE-models involving spatial derivatives of higher order such as the Swift–Hohenberg equation (see Section 6) or the Kuramoto–Sivashinsky equation [55]. Since the expression in the large brackets on the right-hand side of Eq. (17) represent the deterministic part and the stochastic contribution is just an additional term, we find that Eq. (17) also generalizes the stochastic versions of the mentioned PDE-models.

Now inserting the Fourier expansion (3) into (17), multiplying both sides by $\exp(-\mathrm{i}k_n x)$ and integrating over space, we obtain the infinite set of SDEs in the Fourier picture

$$\mathrm{d}u_n(t) = \left[\alpha_n u_n(t) + \beta_n \sum_l u_l(t)u_{n-l}(t) + \gamma_n \sum_{l,m} u_l(t)u_m(t)u_{n-l-m}(t)\right]\mathrm{d}t + \mathrm{d}\Gamma_n(t) \tag{18}$$

similar to (4) with the constants

$$\alpha_n = \mathcal{F}[K_1](k_n), \quad \beta_n = \frac{\mathcal{F}[K_2](k_n)}{\sqrt{|\Omega|}}, \quad \gamma_n = \frac{\mathcal{F}[K_3](k_n)}{|\Omega|}, \tag{19}$$

$\alpha_n = \alpha_{-n}, \beta_n = \beta_{-n}, \gamma_n = \gamma_{-n}$ and $\mathcal{F}[K]$ taken from (13). Recall that $u_n = u_{-n} \in \mathcal{R}$ according to the previous

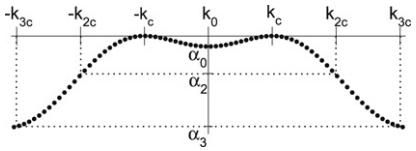

Fig. 1. Illustration of $\alpha_n = \alpha(k_n)$ taken from (19). The stability threshold is given by $\alpha_c = 0$ at k_c, k_{-c}.

sections, which will be taken into account in the following. Further, the terms $\mathrm{d}\Gamma_n$ represent the random fluctuations of the spatial mode u_n, and we find from Section 2 that $\mathrm{d}\Gamma_n(t) = \eta \mathrm{d}W_n(t)$ for uncorrelated fluctuations and $\mathrm{d}\Gamma_n(t) = \eta \mathrm{d}W(t)$ for global fluctuations. Fig. 1 illustrates the typical dependence of the parameters α_n on the discrete wavenumber k_n and shows the critical wavenumber $k_{\pm c}$ with $\alpha_c = 0$. Moreover, the illustration shows values $\alpha_n \ll \alpha_0, \alpha_c$ with $|n| \geq 2c$, i.e. a separation of values α_c, α_0 and $\alpha_n, |n| \geq 2$.

4.2. Intermediate step: Deterministic dynamics and the center manifold

In a first step the dynamics is assumed deterministic, i.e. $\eta = 0$. According to Section 3, the system is stable if $\alpha_n < 0$ for all n, and it is marginally stable at the stability threshold $\alpha_n = 0$ for some $|n| = c$. Hence the set of differential equations (18) splits into critical modes u_c and stable modes $u_{i\neq c}$:

$$\dot{u}_c = \alpha_c u_c + \beta_c \sum_n u_n u_{c-n} + 2\gamma_c u_c^3 + \gamma_c \sum_{\substack{n,m \\ n+m\neq \pm c}} u_n u_m u_{c-n-m} \tag{20}$$

$$\dot{u}_i = \alpha_i u_i + 2\beta_i (u_c u_{i-c} + u_{-c} u_{i+c}) + \beta_i \sum_{n\neq \pm c, i\pm c} u_n u_{i-n} + \gamma_i \sum_{n,m} u_n u_m u_{i-n-m} \quad \forall i \neq \pm c. \tag{21}$$

Here, and in the following, we apply the relation $u_n = u_{-n}$. By virtue of $\alpha_c = 0$ and $\alpha_i < 0, i \neq c$, the deterministic center manifold theorem applies [65] and the stable modes $u_{i\neq c}$ depend on u_c, i.e. $u_i = u_i(u_c)$. Inserting the polynomial ansatz

$$u_i = a_i u_c^2 + b_i u_c^3$$

into Eqs. (20) and (21) with $i \neq \pm c$ and comparing the coefficients of orders u_c^2 and u_c^3, we find

$$a_i = -\frac{2\beta_i(\delta_{i,0} + 2\delta_{i,2c})}{\alpha_i} \to u_0, u_{2c} \sim u_c^2 \tag{22}$$

$$b_i = -\frac{2\beta_i(a_{i-c} + a_{i+c})}{\alpha_i}, \quad i \neq 0, \pm c, \pm 2c \to u_i \sim u_c^3. \tag{23}$$

This brief calculation shows that there exist three classes of mode defined corresponding to their scaling behavior with respect to u_c: the critical mode k_c, the subset of stable modes $\{k_n\}, n = 0, 2c, 3c, \ldots$ from Eq. (22), and the other stable modes $\{k_n\}, n \neq 0, 2c, 3c, \ldots$ from Eq. (23).

Since the distinction of stable and critical modes in (20) and (21) implies small time scales $1/|\alpha_k|, |k| > 2c$, the corresponding modes decrease very fast, i.e. $u_k \approx 0$ for $|k| > 2c$ at large times. This assumption is valid if $\alpha_n \ll \alpha_0, \alpha_c$ with $|n| \geq 2c$ (Fig. 1).

To examine the time scales of the critical and stable modes, let us introduce the scaling factor $\varepsilon > 0$ with

$$\alpha_c \sim O(\varepsilon) \quad , \quad \alpha_{i\neq c}, \beta_i, \gamma_i \sim O(1).$$

In other words, ε is proportional to the magnitude of α_c and thus quantifies the distance from the stability threshold $\alpha_c = 0$. Hence the larger the distance from the stability threshold, i.e. the larger ε, the larger the deviations from the stationary state and thus the stronger the nonlinear effects.

In the following, the system is presumed to evolve around the stability threshold and thus $\varepsilon \ll 1$. According to (22) and (23), the mode amplitudes may be written as $u_c = x\varepsilon^m$, $u_0 = y\varepsilon^{2m}$, $u_{2c} = z\varepsilon^{2m}$, $u_i = w\varepsilon^{3m}$, $i \neq 0, \pm 2c, \pm 3c, \ldots$ for some constant $m \in \mathcal{R}$. Here x, y, z are independent of ε. Inserting these expressions into (20) and (21), we find $m = 1/2$, and thus

$$u_c \sim O(\varepsilon^{1/2}), \quad u_{0,2c} \sim O(\varepsilon), \quad u_i \sim O(\varepsilon^{3/2}) \tag{24}$$

and $\mathrm{d}x/\mathrm{d}t \sim O(\varepsilon)$ and $\mathrm{d}y/\mathrm{d}t, \mathrm{d}z/\mathrm{d}t, \mathrm{d}w/\mathrm{d}t \sim O(1)$. Hence the critical mode evolves on the time scale of order $O(\varepsilon)$, which is slow compared to the stable mode time scale of order $O(1)$. This finding confirms the time scale separation. Let us summarize the latter discussion. The stable modes obey the dynamics of the critical modes on the center manifold just around the stability threshold, while they evolve faster than the critical modes. In physical terms, the slow critical modes enslave the fast stable modes, which in turn obey the dynamics of the critical modes. This dependence is also called the slaving principle, and the circular dependence is known as the circular causality [13].

Taking into account the previous results, the set of mode equations up to order $O(\varepsilon^{3/2})$ reduces to

$$\begin{aligned} \dot{u}_c &= \alpha_c u_c + 2\beta_c u_c (u_0 + u_{2c}) + 2\gamma_c u_c^3 \\ \dot{u}_0 &= \alpha_0 u_0 + 4\beta_0 u_c^2 \\ \dot{u}_{2c} &= \alpha_{2c} u_{2c} + 4\beta_{2c} u_c^2 \\ \dot{u}_i &= \alpha_i u_i + 2\beta_i u_c (u_{i-c} + u_{i+c}) \quad i \neq 0, \pm c, \pm 2c, \ldots \end{aligned} \tag{25}$$

while higher spatial modes $u_{3c}, u_{4c}, \ldots$ have been neglected corresponding to the discussion of Fig. 1.

The following subsections treat uncorrelated and global fluctuations and apply the latter results to reduce the set of SDEs (18) to a single stochastic order parameter equation. Moreover, they explain the application of the stochastic center manifold analysis and the adiabatic elimination in the Fokker–Planck description in detail up to order $O(\varepsilon^{5/2})$.

4.3. Spatially uncorrelated fluctuations at order $O(\varepsilon^{3/2})$

Now let us consider random fluctuations with the intensity $\eta \sim O(\varepsilon)$. Applying the results obtained in the previous paragraphs, Eqs. (25) read

$$\mathrm{d}u_c = \left(\alpha_c u_c + 2\beta_c u_c (u_0 + u_{2c}) + 2\gamma_c u_c^3\right) \mathrm{d}t + \eta \mathrm{d}W_c(t) \tag{26}$$

$$\mathrm{d}u_0 = \left(\alpha_0 u_0 + 4\beta_0 u_c^2\right)\mathrm{d}t + \eta \mathrm{d}W_0(t) \tag{27}$$

$$\mathrm{d}u_{2c} = \left(\alpha_{2c} u_{2c} + 4\beta_{2c} u_c^2\right)\mathrm{d}t + \eta \mathrm{d}W_{2c}(t) \tag{28}$$

at order $O(\varepsilon^{3/2})$. Here the modes $u_i, i \neq 0, \pm c, \pm 2c$ have been neglected as they have small magnitudes of order $O(\varepsilon^{3/2})$ and thus do not affect the evolution of u_c at order $O(\varepsilon^{3/2})$.

4.3.1. The stochastic center manifold analysis

To obtain the stochastic order parameter equation we apply the stochastic center manifold analysis [40,41]. Similar to its deterministic version, this analysis assumes the stochastic center manifold of u_0 and u_{2c} of the form

$$u_0(u_c, t) = h_0(u_c, t) = \sum_{n=2}^{\infty} h_0^{(n)}(u_c, t) \tag{29}$$

$$u_{2c}(u_c, t) = h_{2c}(u_c, t) = \sum_{n=2}^{\infty} h_{2c}^{(n)}(u_c, t) \tag{30}$$

with $h_0^{(n)}, h_{2c}^{(n)} \sim O(\varepsilon^{n/2})$. We point out that the manifold is dependent on time due to the random fluctuations, which contrasts to the deterministic center manifold analysis. Further, the subsequent stochastic manifold analysis is valid for small enough nonlinearities only, i.e. the system should remain in the vicinity of the bifurcation point (see Sections 5 and 6 in [41] for more details). Consequently the analysis is restricted to finite order n. With

$$\mathrm{d}u_0 = \frac{\partial h_0}{\partial u_c}\mathrm{d}u_c + \frac{\partial h_0}{\partial t}\mathrm{d}t, \quad \mathrm{d}u_{2c} = \frac{\partial h_{2c}}{\partial u_c}\mathrm{d}u_c + \frac{\partial h_{2c}}{\partial t}\mathrm{d}t$$

and (29), (30), Eqs. (26)–(28) yield

$$\left(\frac{\partial}{\partial t}\mathrm{d}t - \alpha_0 \mathrm{d}t\right) h_0 = \Big[4\beta_0 u_c^2 - \frac{\partial h_0}{\partial u_c}(\alpha_c u_c + 2\beta_c u_c (h_0 + h_c) + 2\gamma_c u_c^3)\Big]\mathrm{d}t - \eta \frac{\partial h_0}{\partial u_c}\mathrm{d}W_c(t) + \eta \mathrm{d}W_0(t)$$

$$\left(\frac{\partial}{\partial t}\mathrm{d}t - \alpha_{2c}\mathrm{d}t\right) h_{2c} = \Big[4\beta_{2c} u_c^2 - \frac{\partial h_{2c}}{\partial u_c}\left(\alpha_c u_c + 2\beta_c u_c (h_0 + h_c) + 2\gamma_c u_c^3\right)\Big]\mathrm{d}t - \eta \frac{\partial h_{2c}}{\partial u_c}\mathrm{d}W_c(t) + \eta \mathrm{d}W_{2c}(t).$$

These equations have the form

$$\left(\frac{\partial}{\partial t}\mathrm{d}t - \alpha \mathrm{d}t\right) g(u_c, t) = f_1(u_c, t)\mathrm{d}t + f_2(u_c, t)\mathrm{d}W(t),$$

which may be inverted [25,40] to

$$g(u_c, t) = \int_{-\infty}^{t} \mathrm{e}^{\alpha(t-\tau)} f_1(u_c, \tau)\mathrm{d}\tau + \int_{-\infty}^{t} \mathrm{e}^{\alpha(t-\tau)} f_2(u_c, \tau)\mathrm{d}W(\tau).$$

It is important to note that $f_1(u_c, t)$ in the first integral is integrated in time explicitly, while the second term represents a stochastic integral. Now the stochastic center manifold contributions to h_0, h_{2c} are calculated at different orders $O(\varepsilon^n)$. Sorting the resulting terms corresponding to their order, we find at order $O(\varepsilon)$

$$h_0^{(2)}(u_c, t) = -\frac{4\beta_0}{\alpha_0} u_c^2 + \eta Z_0(t), \quad Z_0(t) = \int_{-\infty}^{t} \mathrm{e}^{\alpha_0(t-\tau)}\mathrm{d}W_0(\tau) \tag{31}$$

$$h_{2c}^{(2)}(u_c, t) = -\frac{4\beta_{2c}}{\alpha_{2c}} u_c^2 + \eta Z_1(t), \quad Z_1(t) = \int_{-\infty}^{t} \mathrm{e}^{\alpha_{2c}(t-\tau)}\mathrm{d}W_{2c}(\tau) \tag{32}$$

and at order $O(\varepsilon^{3/2})$

$$h_0^{(3)}(u_c, t) = \frac{8\beta_0 \eta}{\alpha_0} u_c Z_2(t), \quad Z_2(t) = \int_{-\infty}^{t} \mathrm{e}^{\alpha_0(t-\tau)}\mathrm{d}W_c(\tau) \tag{33}$$

$$h_{2c}^{(3)}(u_c, t) = \frac{8\beta_{2c}\eta}{\alpha_{2c}} u_c Z_3(t), \quad Z_3(t) = \int_{-\infty}^{t} \mathrm{e}^{\alpha_{2c}(t-\tau)}\mathrm{d}W_c(\tau). \tag{34}$$

These latter terms define the center manifold (29) and (30), and the stochastic order parameter equation at order $O(\varepsilon^{3/2})$ reads

$$\mathrm{d}u_c = \left(\alpha_c u_c + a u_c^3 + b\eta u_c \left(Z_0(t) + Z_1(t)\right)\right)\mathrm{d}t + \eta \mathrm{d}W_c(t) \tag{35}$$

with $a = 2\gamma_c - 8\beta_0\beta_c/\alpha_0 - 8\beta_{2c}\beta_c/\alpha_{2c}$ and $b = 2\beta_c$. From (35) we learn that the order parameter is subjected both to additive white noise $\mathrm{d}W_c(t)$ and multiplicative noise $Z_0(t), Z_1(t)$. These latter terms represent colored noise with long-memory correlations according to (31) and (32). Since $Z_0(t)$ and $Z_1(t)$ also represent Ornstein–Uhlenbeck processes, Eq. (35) can be extended by the corresponding SDEs

$$\begin{aligned} \mathrm{d}Z_0(t) &= \alpha_0 Z_0 \mathrm{d}t + \mathrm{d}W_0(t), \\ \mathrm{d}Z_1(t) &= \alpha_{2c} Z_1 \mathrm{d}t + \mathrm{d}W_{2c}(t). \end{aligned} \tag{36}$$

In this formulation, the order parameter equation depends on two additional variables Z_0, Z_1, while their evolution equations (35) and (36) are subjected to additive white noise. Moreover, the critical mode u_c and Z_0, Z_1 show the time scale separation of modes as they evolve on the slow and the fast time scale at orders $O(\varepsilon^{3/2})$ and $O(1)$, respectively.

Now let us discuss the statistical properties of the colored noise processes some detail. In the stationary regime, the correlation function of $Z_0(t)$ reads

$$\langle Z_0(t) Z_0(s)\rangle = \frac{1}{|\alpha_0|}\mathrm{e}^{-|\alpha_0||t-s|}, \tag{37}$$

its variance is $\sigma^2 = 1/|\alpha_0|$, and its power spectrum is given by

$$S^2(\omega) = \frac{1}{|\alpha_0|^2 + \omega^2} = \frac{\tau_0^2}{1 + \tau_0^2\omega^2} \tag{38}$$

with $\tau_0 = 1/|\alpha_0|$. Equivalent results may be gained for $Z_1(t)$.

The perfect time scale separation of the spatial modes occurs for $\alpha_0 \to -\infty$, leading to the vanishing time scale of the dynamics τ_0, its variance σ^2 and the power $S^2(\omega)$. Consequently the perfect time scale separation yields $Z_0(t) \to 0$ for $t \to \infty$. This behavior is confirmed by the corresponding stationary probability density $P_s(Z_0) = \delta(Z_0)$, cf. Eq. (15). In this context we mention the studies on colored noise [66, 67], which assume random fluctuations whose strength scales with the dynamical time scale τ_0. These studies presume that $\tau_0 \to 0$ yields the white-noise fluctuations with non-vanishing variance. In contrast, the fluctuations in the present work exhibit both vanishing variance and power spectrum as $\tau_0 \to 0$.

To obtain a single order parameter equation, it is necessary to further reduce the systems (35) and (36). However, the stochastic center manifold approach is not capable to do that as the obtained equation system represents an irreducible form [40]. In other words, re-applying the previous analysis yields the same equation systems (35) and (36). The reason for this behavior is that $Z_0(t)$ and $Z_1(t)$ are independent of u_c and evolve at the order $O(1)$. Thus they are already separated from the mode u_c. Consequently, a different approach is necessary, which does not depend on $Z_0(t)$ and $Z_1(t)$ explicitly. To deal with this problem, Xu and Roberts [40] proposed a center manifold approach taking into account the shape of resulting probability densities similar to the work of Knobloch and Wiesenfeld [22] on Gaussian-like probability densities. Here, however, we aim to find solutions without any assumption on the shape of the probability densities. Our method involves an adiabatic elimination procedure based on the corresponding Fokker–Planck equation to gain a single order parameter equation.

4.3.2. The reduced probability density function

We follow the adiabatic elimination approach of Drolet and Vinal [38,42]. After re-scaling the variables $\bar{u}_c = u_c/\sqrt{\varepsilon}$, $\bar{\eta} = \eta/\varepsilon$, $\bar{\alpha_c} = \alpha_c/\varepsilon$ with $Z_0, Z_1, \alpha_0, a, b \sim O(1)$ according to our previous results (24), the Fokker–Planck equation of Eqs. (35) and (36) reads

$$\begin{aligned}\frac{\partial P(\bar{u}_c, \mathbf{Z}, t)}{\partial t} &= -\frac{\partial}{\partial \bar{u}_c}\left(\bar{\alpha}_c\bar{u}_c + a\bar{u}_c^3 + b\bar{\eta}\bar{u}_c\,(Z_0 + Z_1)\right)\varepsilon P(\bar{u}_c, \mathbf{Z}, t) \\ &\quad - \left(\frac{\partial}{\partial Z_0}(\alpha_0 Z_0) - \frac{\partial}{\partial Z_1}(\alpha_{2c} Z_1)\right) P(\bar{u}_c, \mathbf{Z}, t) \\ &\quad + \bar{\eta}^2 \frac{\partial^2}{\partial \bar{u}_c^2}\varepsilon\, P(\bar{u}_c, \mathbf{Z}, t) + \left(\frac{\partial^2}{\partial Z_0^2} + \frac{\partial^2}{\partial Z_1^2}\right) P(\bar{u}_c, \mathbf{Z}, t)\end{aligned} \tag{39}$$

with $\mathbf{Z} = (Z_0, Z_1)^t$ and the joint probability density $P(\bar{u}_c, \mathbf{Z}, t)$. Then assuming natural boundary conditions and considering the decomposition $P(\bar{u}_c, \mathbf{Z}, t) = P(\bar{u}_c, t)P(\mathbf{Z}|\bar{u}_c, t)$ with the conditional probability density function $P(\mathbf{Z}|\bar{u}_c, t)$, the double integration over $\mathbf{Z}$ yields

$$\begin{aligned}\frac{\partial P(\bar{u}_c, t)}{\partial t} &= -\frac{\partial}{\partial \bar{u}_c}\left[\left(\bar{\alpha}_c\bar{u}_c + a\bar{u}_c^3\right) + b\bar{\eta}\bar{u}_c\,\langle Z_0, Z_1|\bar{u}_c\rangle \right. \\ &\quad \left. + \bar{\eta}^2\frac{\partial^2}{\partial \bar{u}_c^2}\right] P(\bar{u}_c, t)\varepsilon\end{aligned}$$

with

$$\langle Z_0, Z_1|\bar{u}_c\rangle = \int_{-\infty}^{\infty}\int_{-\infty}^{\infty} \mathrm{d}Z_0\mathrm{d}Z_1 (Z_0 + Z_1) P(\mathbf{Z}|\bar{u}_c, t). \tag{40}$$

We learn that the probability density $P(\bar{u}_c, t)$ evolves on the slow time scale of order $O(\varepsilon)$ and is coupled to Z_0, Z_1 by (40). Further, the integration of (39) over $\bar{u}_c$ assuming natural boundary conditions yields the Fokker–Planck equation of the joint probability density function $P(\mathbf{Z}, t)$

$$\begin{aligned}\frac{\partial P(\mathbf{Z}, t)}{\partial t} &= -\left(\frac{\partial}{\partial Z_0}(\alpha_0 Z_0) - \frac{\partial}{\partial Z_1}(\alpha_{2c} Z_1)\right) P(\mathbf{Z}, t) \\ &\quad + \left(\frac{\partial^2}{\partial Z_0^2} + \frac{\partial^2}{\partial Z_1^2}\right) P(\mathbf{Z}, t).\end{aligned}$$

We observe that $P(\mathbf{Z}, t)$ evolves on a fast time scale of order $O(1)$ and is independent of u_c. Hence the time scale separation between u_c and $\mathbf{Z}$ observed in the stochastic differential equations (35) and (36) is retained in the dynamics of the corresponding probability density functions.

By virtue of this time scale separation, we focus on the time scale at order $O(1)$, and gain from Eq. (39)

$$\begin{aligned}\frac{\partial P(\mathbf{Z}|\bar{u}_c, t)}{\partial t} &= -\left(\frac{\partial}{\partial Z_0}(\alpha_0 Z_0) + \frac{\partial}{\partial Z_1}(\alpha_{2c} Z_1)\right) P(\mathbf{Z}|\bar{u}_c, t) \\ &\quad + \left(\frac{\partial^2}{\partial Z_0^2} + \frac{\partial^2}{\partial Z_1^2}\right) P(\mathbf{Z}|\bar{u}_c, t).\end{aligned} \tag{41}$$

Here we approximated $P(\bar{u}_c, t)$ by a constant on the time scale $O(1)$, i.e.

$$\frac{\mathrm{d}P(\bar{u}_c, \mathbf{Z}, t)}{\mathrm{d}t} \approx P(\bar{u}_c, t)\frac{\mathrm{d}P(\mathbf{Z}|\bar{u}_c, t)}{\mathrm{d}t},$$

which reflects the idea of an adiabatic behavior. In other words, the dynamics of $P(\bar{u}_c, t)$ is much slower than the dynamics on the time scale $O(1)$ and thus may be treated as stationary. Then the stationary solution of (41) on the time scale $O(1)$ reads

$$P_s(\mathbf{Z}|u_c) = \frac{\sqrt{|\alpha_0||\alpha_{2c}|}}{2\pi}\mathrm{e}^{-|\alpha_0|Z_0^2/2 - |\alpha_{2c}|Z_1^2/2}. \tag{42}$$

Since $P(\mathbf{Z}, t)$ approaches its stationary state much faster than $P(\bar{u}_c, t)$, we can apply Eq. (42) in Eq. (40) as a good approximation and obtain

$$\langle \mathbf{Z}|\bar{u}_c\rangle = \int_{-\infty}^{\infty}\int_{-\infty}^{\infty} \mathrm{d}Z_0\mathrm{d}Z_1\,(Z_0 + Z_1)\,P_s(\mathbf{Z}|\bar{u}_c) = 0.$$

Hence the probability density function of the order parameter obeys

$$\begin{aligned}\frac{\partial P(u_c, t)}{\partial t} &= -\frac{\partial}{\partial u_c}\left(\alpha_c u_c + a u_c^3\right) P(u_c, t) \\ &\quad + \eta^2\frac{\partial^2}{\partial u_c^2} P(u_c, t)\end{aligned} \tag{43}$$

with the stationary solution

$$P_s(u_c) = \mathcal{N} \mathrm{e}^{-(\alpha_c u_c^2 + a u_c^4/2)/2\eta^2} \tag{44}$$

and the normalization constant $\mathcal{N}$. We observe that the stationary probability density exhibits maxima x_m at the roots of $\alpha_c x_m + a x_m^3 = 0$. The stationary solution in Eq. (44) is well-known in literature and describes a pitchfork bifurcation subject to additive random fluctuations, see e.g. [16]. Hence the previous analysis steps reproduce the well-known results.

To gain further insights to the effects of spatially uncorrelated fluctuation on the bifurcation structure, a possible subsequent step could extract the order parameter equation at higher nonlinear order. For instance, the system of stochastic differential equations at order $O(\varepsilon^{5/2})$ reads

$$\begin{aligned}
\mathrm{d}u_c &= (\alpha_c + b(u_0 + u_{2c})u_c + \gamma_c(2u_c^3 + (4u_{2c}^2 + 3u_0^2)u_c \\
&\quad + 6u_c u_0 u_{2c}))\mathrm{d}t + \eta \mathrm{d}W_c(t) \\
\mathrm{d}u_0 &= (\alpha_0 u_0 + 4\beta_0 u_c^2 + \beta_0(u_0^2 + 2u_{2c}^2) \\
&\quad + 2\gamma_0(u_0 + u_{2c})u_c^2)\mathrm{d}t + \eta \mathrm{d}W_0(t) \\
\mathrm{d}u_{2c} &= (\alpha_{2c} u_0 + 4\beta_{2c} u_c^2 + 2u_0 u_{2c} + \gamma_{2c} u_c^2(2u_{2c} + u_0))\mathrm{d}t \\
&\quad + \eta \mathrm{d}W_{2c}(t).
\end{aligned} \tag{45}$$

First calculations show that further different colored-noise processes occur, which render the proposed analytical procedure much more complex than at order $O(\varepsilon^{3/2})$. However, preliminary numerical investigations of Eq. (45) do not show a change of the bifurcation structure subject to the random fluctuations; see the comparison of orders $O(\varepsilon^{3/2})$ and $O(\varepsilon^{5/2})$ in Fig. 5. In addition, the detailed investigation of uncorrelated fluctuations would exceed the major aim of the work and thus we do not go into more detail here.

Summarizing, this subsection introduced the stochastic center manifold approach and the adiabatic elimination procedure for the Fokker–Planck equation. Now the following subsection applies the same combination of both methods to gain insights into nonlinear effects in the presence of global fluctuations. We shall observe that the analytical calculations are less complex and thus allow for the analytical study of high orders of ε.

4.4. Spatially global fluctuations at order $O(\varepsilon^{3/2})$

Now considering global fluctuations, the new focus of this section is the critical mode u_c and the stable mode u_0, while neglecting all other modes. This represents a reasonable approximation if $\alpha_0 \gg \alpha_{2c}, \alpha_{3c}, \ldots$ (cf. the discussion of Fig. 1) and allows us to clarify some nonlinear effects. To learn more about the error made by this approximation, Sections 5 and 6 show numerical studies which compare results from two modes u_c, u_0 and three modes u_c, u_0, u_{2c}. It will turn out that both approximations yield qualitatively similar results.

Considering global fluctuations, the evolution equations (18) read

$$\mathrm{d}u_c = \left(\alpha_c u_c + 2\beta_c u_c u_0 + 2\gamma_c u_c^3\right)\mathrm{d}t \tag{46}$$

$$\mathrm{d}u_0 = \left(\alpha_0 u_0 + 4\beta_0 u_c^2\right)\mathrm{d}t + \eta \mathrm{d}W(t). \tag{47}$$

Similar to the previous section, the stochastic center manifold u_0 is modeled by

$$u_0(u_c, t) = h_0(u_c, t) = \sum_{n=2}^{\infty} h_0^{(n)}(u_c, t)$$

and the lowest contributions to the stochastic center manifolds are computed as

$$h_0^{(2)} = -\frac{4\beta_0}{\alpha_0} u_c^2 + \eta Z_0(t), \quad Z_0(t) = \int_{-\infty}^{t} \mathrm{e}^{\alpha_0(t-\tau)} \mathrm{d}W(\tau)$$

$$h_0^{(3)} = 0.$$

Then the order parameter equation at order $O(\varepsilon^{3/2})$ reads

$$\mathrm{d}u_c = \left(\alpha_c u_c + a u_c^3 + b\eta u_c Z_0(t)\right)\mathrm{d}t.$$

We observe that the order parameter is subjected to the multiplicative random fluctuations $Z_0(t)$, which represent an Ornstein–Uhlenbeck process. Subsequently, we find the equation system

$$\begin{aligned}
\mathrm{d}u_c &= \left(\alpha_c u_c + a u_c^3 + b u_c Z_0\right)\mathrm{d}t, \\
\mathrm{d}Z_0 &= \alpha_0 Z_0 \mathrm{d}t + \mathrm{d}W(t),
\end{aligned} \tag{48}$$

which is irreducible, as in the previous section.

To obtain a single order parameter equation, we apply the adiabatic elimination procedure introduced in the previous section. After re-scaling the variables similarly to the previous section, the Fokker–Planck equation corresponding to Eqs. (48) reads

$$\begin{aligned}
&\frac{\partial P(\bar{u}_c, Z_0, t)}{\partial t} \\
&= -\frac{\partial}{\partial \bar{u}_c}\left(\bar{\alpha_c}\bar{u}_c + a\bar{u}_c^3 + b\bar{\eta}\bar{u}_c Z_0\right)\varepsilon P(\bar{u}_c, Z_0, t) \\
&\quad - \frac{\partial}{\partial Z_0}(\alpha_0 Z_0)\, P(\bar{u}_c, Z_0, t) + \frac{\partial^2}{\partial Z_0^2} P(\bar{u}_c, Z_0, t).
\end{aligned} \tag{49}$$

Assuming natural boundary conditions, the integration over Z_0 yields

$$\begin{aligned}
\frac{\partial P(\bar{u}_c, t)}{\partial t} &= -\frac{\partial}{\partial \bar{u}_c}\left[\left(\bar{\alpha_c}\bar{u}_c + a\bar{u}_c^3\right) + b\bar{\eta}\bar{u}_c \langle Z_0|\bar{u}_c\rangle\right] \\
&\quad \times P(\bar{u}_c, t)\varepsilon
\end{aligned} \tag{50}$$

with

$$\langle Z_0|\bar{u}_c\rangle = \int_{-\infty}^{\infty} \mathrm{d}Z_0 Z_0 P(Z_0|\bar{u}_c, t). \tag{51}$$

Here we set $P(\bar{u}_c, Z_0, t) = P(Z_0|\bar{u}_c, t)P(\bar{u}_c, t)$. From Eq. (50), we learn that $P(\bar{u}_c, t)$ evolves on a slow time scale of order $O(\varepsilon)$. Moreover, the integration of Eq. (49) over u_c with natural boundary conditions yields

$$\frac{\partial P(Z_0, t)}{\partial t} = -\frac{\partial}{\partial Z_0}(\alpha_0 Z_0)\, P(Z_0, t) + \frac{\partial^2}{\partial Z_0^2} P(Z_0, t).$$

Thus $P(Z_0, t)$ evolves on a fast time scale of order $O(1)$. By virtue of this time scale separation, we apply the adiabatic

approximation $P(\bar{u}_c, t) = \text{const}$ at time scale $O(1)$ and find

$$\frac{\partial P(Z_0|\bar{u}_c, t)}{\partial t} = -\frac{\partial}{\partial Z_0}(\alpha_0 Z_0)\, P(Z_0|\bar{u}_c, t) + \frac{\partial^2}{\partial Z_0^2} P(Z_0|\bar{u}_c, t), \tag{52}$$

with the stationary solution

$$P_s(Z_0|u_c) = \frac{|\alpha_0|}{\sqrt{2\pi}} \mathrm{e}^{-|\alpha_0| Z_0^2/2}. \tag{53}$$

Then Eq. (51) is computed to $\langle Z_0|\bar{u}_c\rangle = 0$ and the probability density function of the order parameter obeys

$$\frac{\partial P(\bar{u}_c, T)}{\partial T} = -\frac{\partial}{\partial \bar{u}_c}\left(\bar{\alpha_c}\bar{u}_c + a\bar{u}_c^3\right) P(\bar{u}_c, T) \tag{54}$$

on a large time scale with $T = \varepsilon t$. Eq. (54) considers terms of order $O(\varepsilon)$, which is different from the order $O(\varepsilon^{3/2})$ of the corresponding SDE. The following paragraphs will pay attention to this distinction of orders in ε as it guarantees the treatment of all contributing terms.

Eq. (54) is equivalent to the order parameter equation

$$\dot{u}_c = \alpha_c u_c + 2\gamma_c u_c^3, \tag{55}$$

which is deterministic. Subsequently, the stationary probability density exists for $\gamma_c < 0$, and reads

$$P_s(u_c) = \sum_n A_n \delta(u_c - x_n) \tag{56}$$

while A_n are normalization constants and x_n are the stationary solutions of $\alpha_c x_n + a x_n^3 = 0$.

4.5. Spatially global fluctuations at order $O(\varepsilon^2)$

Now let us study global random fluctuations at the higher order $O(\varepsilon^2)$ while neglecting the amplitudes $u_{2c}, u_{3c}, \ldots$ similar to the previous sections. In comparison to order $O(\varepsilon^{3/2})$, now the SDE of the stable mode u_0 exhibits additional terms, and we obtain

$$\mathrm{d}u_c = \left(\alpha_c + b u_0 u_c + 2\gamma_c u_c^3\right)\mathrm{d}t \tag{57}$$

$$\mathrm{d}u_0 = \left(\alpha_0 u_0 + 4\beta_0 u_c^2 + \beta_0 u_0^2 + 2\gamma_0 u_0 u_c^2\right)\mathrm{d}t + \eta \mathrm{d}W(t). \tag{58}$$

The subsequent application of the stochastic center manifold analysis retains the lower order terms $h_0^{(2)}$ and $h_0^{(3)}$ and yields the additional term

$$h_0^{(4)}(u_c) = \beta_0\eta^2 Z_5 - 8\frac{\beta_0\alpha_c}{\alpha_0^2}u_c^2 + 4\frac{B}{b}\eta Z_4 u_c^2 + A u_c^4$$

with the colored random fluctuations

$$Z_4(t) = \int_{-\infty}^{t} \mathrm{e}^{\alpha_0(t-\tau)} Z_0(\tau)\mathrm{d}\tau,$$

$$Z_5(t) = \int_{-\infty}^{t} \mathrm{e}^{\alpha_0(t-\tau)} Z_0^2(t)\mathrm{d}\tau.$$

Now the stochastic center manifold reads

$$u_0(u_c, t) = -\frac{4\beta_0}{\alpha_0}u_c^2 + \eta Z_0(t) + h_0^{(4)},$$

leading to

$$\mathrm{d}u_c = \left[\left(\alpha_c + b\eta Z_0 + \beta_0 b\eta^2 Z_5(t)\right)u_c + \left(2\gamma_c - 4\frac{b\beta_0}{\alpha_0} - 8\frac{\beta_0 b\alpha_c}{\alpha_0^2} + B\eta Z_4(t)\right)u_c^3 - A u_c^5\right]\mathrm{d}t$$

$$\mathrm{d}Z_0 = \alpha_0 Z_0 \mathrm{d}t + \mathrm{d}W$$

$$\mathrm{d}Z_4 = (\alpha_0 Z_4 + Z_0)\mathrm{d}t$$

$$\mathrm{d}Z_5 = (\alpha_0 Z_5 + Z_0^2)\mathrm{d}t$$

with the variables A, B defined in the Appendix.

First let us study some statistical properties of Z_4 and Z_5. We find

$$\langle Z_4(t)\rangle = 0, \quad \langle Z_4(t) Z_4(T)\rangle = \frac{\mathrm{e}^{-|\alpha_0||T-t|}(1+2\alpha_0)}{4\alpha_0^2|\alpha_0|} \tag{59}$$

for $|T - t| \to \infty$. The comparison of (59) and (37)reveals similar first and second cumulants of Z_4 and Z_0 and thus allows us to assume $Z_4 \approx Z_0/2\alpha_0$ for $|\alpha_0| \ll 1$. This latter approximation has been discussed in Fig. 1.

Correspondingly, we find the expressions

$$\langle Z_5(t)\rangle = \frac{1}{\alpha_0^2},$$
$$\langle (Z_5(T) - \langle Z_5\rangle)\rangle = \frac{2\mathrm{e}^{-|\alpha_0||T-t|}}{3\alpha_0^4}(2 - \mathrm{e}^{\alpha(|T-t|)}) \tag{60}$$

with the statistical second cumulant $\left\langle (Z_5(t) - \langle Z_5\rangle)^2\right\rangle = 2/3\alpha_0^4$. Then Z_5 and Z_0 share the first and second statistical cumulant if $Z_5 \approx \sqrt{2/3|\alpha_0|^3}Z_0 + 1/\alpha_0^2$, which is a valid approximation up to second order statistics.

Then utilizing these approximations, the corresponding Fokker–Planck equation reads

$$\frac{\partial P(\bar{u}_c, Z_0, t)}{\partial t} = -\frac{\partial}{\partial \bar{u}_c}\left[\left(\bar{\alpha_c}\bar{u}_c + a\bar{u}_c^3 + b\bar{\eta}\bar{u}_c Z_0\right)\varepsilon + \left(\frac{B}{2\alpha_0}\bar{\eta} Z_0 \bar{u}_c^3 - 8\frac{\beta_0 b\bar{\alpha_c}}{\alpha_0^2}\bar{u}_c^3 + \beta_0 b\bar{\eta}^2 Z_5(Z_0) + A\bar{u}_c^5\right)\varepsilon^2\right] \times P(\bar{u}_c, Z_0, t) - \frac{\partial}{\partial Z_0}(\alpha_0 Z_0)\, P(\bar{u}_c, Z_0, t) + \frac{\partial^2}{\partial Z_0^2} P(\bar{u}_c, Z_0, t) \tag{61}$$

with $Z_5(Z_0) = \sqrt{2/3\alpha_0^3}Z_0 + 1/\alpha_0^2$. In addition, again we find $\partial P(Z_0)/\partial t \sim O(1)$ as in the previous section and we obtain

$$\frac{\partial P(\bar{u}_c, t)}{\partial t} = -\frac{\partial}{\partial \bar{u}_c}\left[\left(\bar{\alpha_c}\bar{u}_c + a\bar{u}_c^3\right)\varepsilon + \beta_0 b\bar{\eta}^2 \langle Z_5\rangle \varepsilon^2 + \left(8\frac{\beta_0 b\bar{\alpha_c}}{\alpha_0^2}\bar{u}_c^3 - A\bar{u}_c^5\right)\varepsilon^2\right] P(\bar{u}_c, t). \tag{62}$$

Eq. (62) shows that $P(\bar{u}_c, t)$ evolves on two time scales at orders $O(\varepsilon)$, $O(\varepsilon^2)$, and thus is slower than $P(Z_0, t)$. Consequently the adiabatic approximation $P(\bar{u}_c, Z_0, t) \approx P_s(Z_0|\bar{u}_c)P(\bar{u}_c, t)$ is valid at the time scales of orders $O(\varepsilon)$, $O(\varepsilon^2)$ with $P_s(Z_0|u_c)$ taken from (53).

The Fokker–Planck equation (62) does not contain all terms of order $O(\varepsilon^2)$, though some of these terms occur. This will be seen in the subsequent section, which treats a higher order. However, (62) contains all terms at order $O(\varepsilon^{3/2})$ as we increased the order of terms compared to the previous section. Consequently, we treat (62) in the order $O(\varepsilon^{3/2})$ and obtain

$$\frac{\partial P(u_c)}{\partial t} = -\frac{\partial}{\partial u_c}\left(\alpha_c u_c + a u_c^3\right) P(u_c)$$

with the stationary solution

$$P_s(u_c) = \sum_n A_n \delta(u_c - x_n) \tag{63}$$

while A_n are normalization constants and x_n are the deterministic stationary solutions with $\alpha_c x_n + a x_n^3 = 0$. This solution is the same as in the previous section at order $O(\varepsilon^{3/2})$.

To gain all terms at order $O(\varepsilon^2)$ in the Fokker–Planck equation, we have to further increase the order in the SDE. Essentially this additional treatment of higher order guarantees the valid investigation of highly nonlinear effects and yields a novel effect.

4.6. Spatially global fluctuations at orders $O(\varepsilon^{5/2})$

At this order an additional term occurs in the equation of the critical mode u_c compared to the previous section, and it is

$$\mathrm{d}u_c = \left(\alpha_c + b u_0 u_c + 2\gamma_c u_c^3 + 3\gamma_c u_c u_0^2\right)\mathrm{d}t \tag{64}$$

$$\mathrm{d}u_0 = \left(\alpha_0 u_0 + 4\beta_0 u_c^2 + \beta_0 u_0^2 + 2\gamma_0 u_0 u_c^2\right)\mathrm{d}t + \eta \mathrm{d}W(t). \tag{65}$$

Then the subsequent stochastic center manifold analysis yields $h_0^{(5)}(u_c, t) = 0$ and

$$\begin{aligned}\mathrm{d}u_c \;=\; & \Bigg[\left(\alpha_c + b\eta Z_0 + \beta_0 b\eta^2 Z_5 - 3\gamma_c \eta^2 Z_0^2\right) u_c \\ & - \left(A + 48\gamma_c \frac{\beta_0^2}{\alpha_0^2}\right) u_c^5 + \Bigg(2\gamma_c - 4\frac{b\beta_0}{\alpha_0} - 8\frac{\beta_0 b\alpha_c}{\alpha_0^2} \\ & + \left(\frac{B}{2\alpha_0} - 24\frac{\gamma_c\beta_0}{\alpha_0}\right)\eta Z_0\Bigg) u_c^3\Bigg]\mathrm{d}t\end{aligned}$$

$$\mathrm{d}Z_0 = \alpha_0 Z_0 \mathrm{d}t + \mathrm{d}W_0$$

$$\mathrm{d}Z_4 = (\alpha_0 Z_4 + Z_0)\mathrm{d}t$$

$$\mathrm{d}Z_5 = (\alpha_0 Z_5 + Z_0^2)\mathrm{d}t.$$

Applying the approximations of $Z_4(t)$ and $Z_5(t)$ from the previous section, the final Fokker–Planck equation for the order parameter reads at order $O(\varepsilon^2)$

$$\frac{\partial P(u_c)}{\partial t} = -\frac{\partial}{\partial u_c}\left[\left(\alpha_c - \alpha_{th}(\eta)\right) u_c + C u_c^3 + D u_c^5\right] P(u_c) \tag{66}$$

with

$$\alpha_{th}(\eta) = \eta^2\left(\frac{\beta_0 b}{\alpha_0^2} - 3\frac{\gamma_c}{|\alpha_0|}\right) \tag{67}$$

and the constants C, D defined in the Appendix.

We observe that the order parameter u_c obeys the deterministic equation

$$\dot{u}_c = \left(\alpha_c - \alpha_{c,th}(\eta)\right) u_c + C u_c^3 + D u_c^5. \tag{68}$$

Further, α_{th} defines the new stability threshold, which depends on the fluctuation strength η, and thus reflects noise-induced transitions. To our best knowledge Eq. (68) has not been derived yet for additive random fluctuations in general evolution equations. In the case $\alpha_{th} > 0$, the noise retards the emergence of the bifurcation with increasing α_c and thus stabilizes the neural field. From a physical point of view, the global fluctuations represent an external stimulus which forces the system to obey the stimulus dynamics. The stronger the stimulus is, i.e. the larger the fluctuation strength η, the stronger the spatial mode $k = 0$ is, and thus the smaller the contribution of the unstable mode $k = k_c$.[1]

Moreover, the stationary probability density of (66) exists if $D < 0$ and reads

$$P_s(u_c) = \sum_n A_n \delta(u_c - x_{\mathrm{stat}}) \tag{69}$$

with the normalization constants A_n and the deterministic stationary solutions x_n of Eq. (68), which depends on the fluctuation strength η. We remark that Eq. (66) contains all terms of order $O(\varepsilon^2)$.

The following section studies two specific spatial systems which involve different local dynamics and spatial interactions. We compare the analytical results obtained in the current section with the numerical results gained by numerical integration of the set of stochastic mode equations at different orders and the full model (1).

5. Application to a neural field equation

In this section, the model under study describes mathematically the membrane potential $U(x, t)$ of a spatially extended neural population at the location x at time t [53,54]. The following specific model is motivated by the orientation selectivity in the visual cortex [68,10] and assumes local excitation–lateral inhibition interaction with

$$K(x) = \mathcal{N}\frac{a_e}{\sigma_e}\mathrm{e}^{-x^2/2\sigma_e^2}, \quad L(x) = -\mathcal{N}\frac{a_i}{\sigma_i}\mathrm{e}^{-x^2/2\sigma_i^2} \tag{70}$$

defined on the interval $x \in [-\pi/0.65, \pi/0.65]$ with periodic boundary conditions. In other words, the spatial domain Ω is a circle with circumference $|\Omega| = 2\pi/0.65$. Further, a_e and a_i denote the excitatory and inhibitory total synaptic weight, respectively, while σ_e and σ_i represent the range of the

[1] In this context the authors appreciate interesting discussions with A. Neiman.

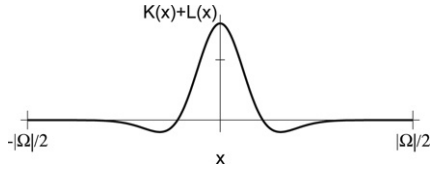

Fig. 2. Effective spatial interaction kernel with the $|\Omega|$-periodic variable x taken from (70). Parameters are $a_e = 1.83$, $a_i = 1.23$, $\sigma_e = 0.2\pi$, $\sigma_i = 0.3\pi$.

corresponding spatial interaction. The constant $\mathcal{N}$ guarantees the normalization of the kernels to $\int_\Omega \mathrm{d}x\, K(x)+L(x) = a_e - a_i$. Fig. 2 shows the effective interaction kernel $K(x) + L(x)$. Further, we presume equal sigmoidal functionals $S_K[U] = S_L[U] \equiv S[U] = 1/(1 + \exp(-5.5(U - 3.0)))$ and choose the local dynamics as $h[U] = -U$. Considering the external input $I(x,t) = I_0 + \Gamma(x,t)$ with the external random fluctuations $\Gamma(x,t)$, the evolution equation under study reads

$$\mathrm{d}U(x,t) = \left(-U(x,t) + \int_\Omega \mathrm{d}y\ (K(x-y) + L(x-y)) \times S[U(y,t)] + I_0\right)\mathrm{d}t + \mathrm{d}\Gamma(x,t). \tag{71}$$

Fig. 3(a) shows the stationary solutions of Eq. (10) subject to the parameter I_0, cf. Eq. (10). We observe the monotonic relation of I_0 to U_0.

Then considering small deviations from the stationary solution U_0, the expansion coefficients in (19) read

$$\alpha_n = S' J_n - 1, \quad \beta_n = \frac{S''}{\sqrt{|\Omega|}} J_n, \quad \gamma_n = \frac{S'''}{6|\Omega|} J_n$$

$$J_n = \left(\frac{a_e I_n(\sigma_e)}{\sigma_e} - \frac{a_i I_n(\sigma_i)}{\sigma_i}\right),$$

$$I_n(\sigma) = 2\mathcal{N} \int_0^{|\Omega|/2} \mathrm{e}^{-x^2/2\sigma^2} \cos(k_n x)\mathrm{d}x,$$

with $I_n(\sigma) > 0$ and $S' = \mathrm{d}S/\mathrm{d}U$, $S'' = \mathrm{d}^2S/\mathrm{d}U^2$, $S''' = \mathrm{d}^3S/\mathrm{d}U^3$ computed at the stationary state U_0; see Fig. 3(b). We observe in Fig. 3(b) that the sign of S', S'' and S''' changes with U_0, which correspondingly may yield sign changes in α_n, β_n and γ_n. Subsequently the stationary state U_0 affects α_n, β_n and γ_n. This behavior of parameters contrasts with most pattern formation studies which exhibit a single varying parameter. However, the specific choice of the parameters guarantees $\beta_n \leq 0$, $\gamma_n < 0$, and thus the stability of the system depends on α_n only. Since α_n defines the linear stability of the system it serves as the control parameter.

Fig. 4 shows the values of α_n as a function of k_n and we observe that $U = 3.1$ guarantees the stability of the system, i.e. $\alpha_n < 0$. The case $U_0 = 3.0$ yields $\alpha_c > 0$, and a single spatial mode with wavenumber $|k| = k_c$ becomes unstable.

5.1. Spatially uncorrelated fluctuations in the mode equations

First we study the effect of uncorrelated fluctuations at various orders in ε. Recall that the control parameter α_c depends on the stationary state U_0 and $\alpha_c \sim \varepsilon$. Thus ε is proportional to the distance from the stability threshold. This study yields some information on the validity of the approximation made in Section 4.3 at order $O(\varepsilon^{3/2})$ compared to order $O(\varepsilon^{5/2})$.

We apply the stochastic Euler forward algorithm with time step $\mathrm{d}t = 0.01$ for the amplitudes $u_c(t)$, u_0 and u_{2c} in Eq. (45) at order $O(\varepsilon^{5/2})$ with the initial values of the modes taken from a uniform distribution in the interval $[-0.4; 0.4]$. Subsequently the stationary probability density $P_s(u_c)$ was computed by an ensemble average over 1000 simulated paths, which showed stationary behavior after 4×10^5 time steps.

To gain some insight into how well the order $O(\varepsilon^{3/2})$ approximates the dynamics of the system compared to the higher order $O(\varepsilon^{5/2})$, Fig. 5 compares the numerical results at order $O(\varepsilon^{5/2})$ and the analytical results in Eq. (44) at lower order $O(\varepsilon^{3/2})$. We observe a good accordance of the results at low fluctuation strengths, and some differences at higher fluctuation strengths. Hence the lower order $O(\varepsilon^{3/2})$ is sufficient for small fluctuation strengths, while higher fluctuation strengths make necessary higher orders in ε.

5.2. Spatially global fluctuations in the mode equations

Now let us investigate the effects of global fluctuations numerically. First the section compares the analytical results to the numerical results gained by stochastic integration of mode equations at different orders. In addition we compare the analytical results for $P(u_c)$ obtained from the two modes u_0 and u_c with numerical results from the mode equations Eq. (18) which have not been reduced by center manifold reduction and the adiabatic elimination. Further, to obtain some insight into the validity of such a restriction to two modes, we compare the $P(u_c)$ from two modes with the $P(u_c)$ from three modes u_0, u_c and u_{2c}. Since $P(u_c)$ has not been determined analytically

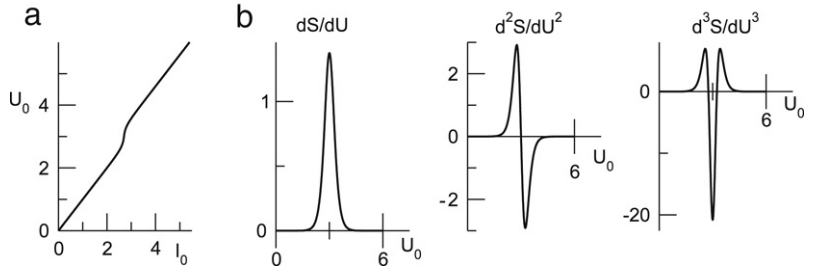

Fig. 3. The stationary solution U_0 and its effect to the sigmoidal derivatives. Panel (a) shows the stationary solutions of Eq. (71), while (b) presents the derivatives of S. See text for the definition of S and Fig. 2 for additional parameters.

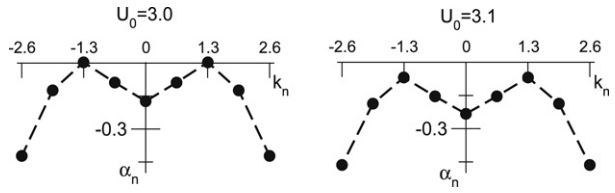

Fig. 4. Values of the control parameter α_n with respect to the wavenumbers k_n for two stationary states U_0. The wavenumbers are discrete with $k_n = n\,2\pi/|\Omega| = 0.65\,n, n \in \mathcal{Z}_0$ and the critical wavenumber is $k_c = 1.3$. The dashed line just illustrates the curve $\alpha_n = \alpha_n(k_n)$, while the filled dots represent values of α_n. Further parameters are defined in Fig. 2.

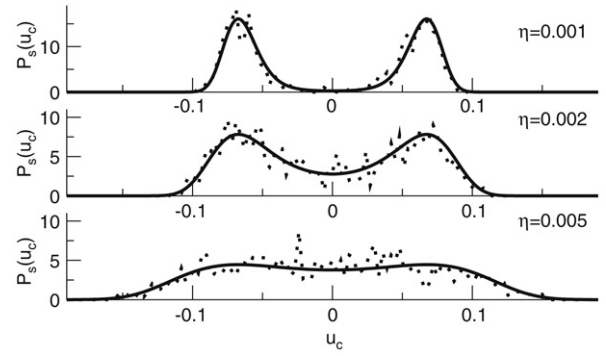

Fig. 5. The stationary probability density $P_s(u_c)$ in the presence of uncorrelated fluctuations for three fluctuation strengths η. The panels show $P_s(u_c)$ at order $O(\varepsilon^{5/2})$ computed by stochastic integration of Eqs. (45) (dotted lines) and the analytical solution $P_s(u_c)$ from Eq. (44) at the lower order $O(\varepsilon^{3/2})$ (solid lines). We choose the stationary state $U_0 = 3.0$, and other parameters are as in Fig. 2.

for three modes, we compare the numerical results from Eq. (18) for three modes to the results from two modes. Then the numerical results from the integration of the full system are compared to the results from the mode equations.

First let us focus on the modes u_c and u_0 at order $O(\varepsilon^{3/2})$. The application of the temporal integration to Eqs. (46) and (47) yields the stationary probability density $P_s(u_c)$ (Fig. 6(a) and (b)). For the stationary state $U_0 = 3.1$ with $\alpha_c < 0$ we find a very narrow probability density $P_s(u_c)$ with maximum at $u_c = 0$ (Fig. 6(a)) reflecting the systems stability. This result shows good accordance to the analytical result (56). In the case of $U_0 = 3.0$, i.e. $\alpha_c > 0$, the spatially constant stationary state is unstable, and we find a bimodal probability density $P(u_c)$ with sharp peaks at $u_c = \pm x_0$ (Fig. 6(b)). In other words, the system is governed by the spatial modes with wavenumber $\pm k_c$ and thus exhibits a periodic pattern with wavelength $2\pi/k_c$. The comparison to the analytical result (56) also shows good accordance as the values x_0 coincide with the analytical stationary solution $x_n = \pm\sqrt{-\alpha_c/2\gamma_c}$. These results confirm our analysis steps in Section 4.

In Section 4.4 we approximated the set of mode equations by the u_0 and u_c. To gain some insight into the validity of this approximation, Fig. 6(c) and (d) present numerical results for $P(u_c)$ by considering additionally the mode u_{2c}, i.e. the spatial modes u_c, u_0, u_{2c}. We observe a good accordance to the analytical results obtained from two spatial modes (Fig. 6(a) and (b)). Consequently no novel effects occur at low orders $O(\varepsilon^{3/2})$ and correspondingly at order $O(\varepsilon^2)$, as the analysis has shown. Further, Fig. 7 presents the bifurcation diagram computed from the analytical solution (55), and we observe the pitchfork bifurcation well-known from the deterministic case [69,70]. We point out that the bifurcation structure is not affected by the fluctuation strength η.

Now let us focus on the next higher order $O(\varepsilon^{5/2})$. Fig. 8 shows the stationary probability density $P_s(u_c)$ obtained by the stochastic integration of Eqs. (64) and (65) for two modes u_c, u_0 (Fig. 8(a) and (b)). For $U_0 = 3.1$, $\alpha_c < 0$, yielding the numerical result $P_s(u_c) = \delta(u_c)$ (Fig. 8(a)), which coincides with the analytical result from Eq. (63). Moreover, numerical integrations for $U_0 = 3.0$, i.e. $\alpha_c > 0$, yield stationary probability density functions which depend on the fluctuation strength η (Fig. 8(b)): the larger the fluctuation strength η the lower the values of the stationary solution of u_c. This behavior also shows good accordance with the analytical result (63), which predicts deterministic dynamics of the type

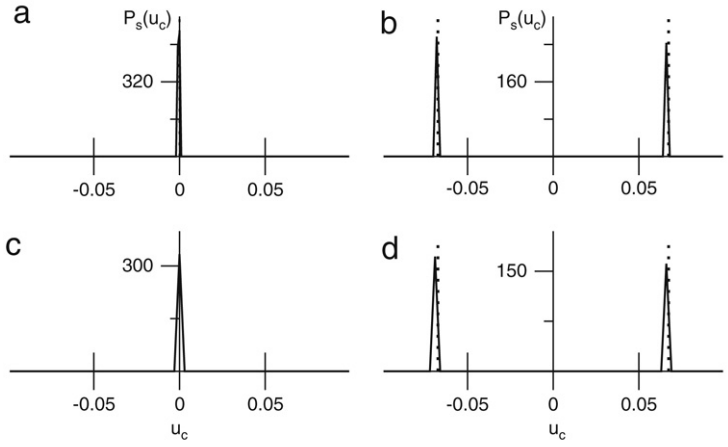

Fig. 6. The stationary probability density $P_s(u_c)$ computed for global fluctuations at orders $O(\varepsilon^{3/2})$ at two different values U_0 and for different numbers of modes. The top row shows $P_s(u_c)$ computed from Eqs. (46), (47) for (a) $U_0 = 3.1$ with $\alpha_c < 0$ and (b) $U_0 = 3.0$ with $\alpha_c > 0$. The bottom row shows $P_s(u_c)$ computed from Eqs. (18) for (c) $U_0 = 3.1$ and (d) $U_0 = 3.0$. The vertical dotted lines represent the stationary states obtained from (56). Other parameters are $\eta = 0.02$ and are taken from Figs. 2 and 4.

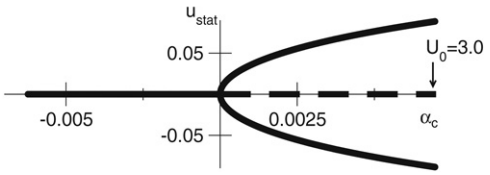

Fig. 7. The bifurcation diagram of the order parameter equation at orders $O(\varepsilon^{3/2})$, $O(\varepsilon^2)$ for global fluctuations corresponding to Eq. (55) with $u_{\text{stat}} = u_n$. Solid lines denote stable stationary states, whereas unstable stationary states are encoded by dashed lines. The diagram is independent of η, and further parameters are taken from Figs. 2 and 4.

$P(u_c) = a\delta(u_c - x_0) + b\delta(u_c + x_0)$, where x_0 depends on the fluctuation strength η. These findings confirm the analysis steps in Section 4. However, the numerically computed probability density functions exhibit a non-vanishing width which contrasts with the analytical results. Extended numerical simulation studies with longer integration times or smaller time step dt confirm the probability densities in Fig. 8. Consequently the non-vanishing width of $P_s(u_c)$ seen numerically is likely a feature of the approximations in the theory. Since the analytical results at lower orders $O(\varepsilon^{3/2})$, $O(\varepsilon^2)$ have been confirmed in the last paragraphs, the strong approximations of Z_4 and Z_5 in Section 4.5 cause these difference of results.

Finally we integrated the stochastic differential equations (18) for the spatial modes u_c, u_0 and u_{2c} and found good agreement with the results from two modes u_c and u_0; see Fig. 8(c) and (d). Consequently the analytical treatment of two modes is sufficient to reveal this shift. In addition, Fig. 9 presents the corresponding bifurcation diagram for two fluctuation strengths, and we observe a delayed pitchfork bifurcation for $\eta > 0$.

Figs. 8 and 9 reveal a delayed transition by global fluctuations, which stabilize the system. This shift of the critical parameter α_c to higher values is given by $\alpha_{th} > 0$, cf. Eq. (67), which depends on the variables $\alpha_0, \beta_0, \beta_c$ and γ_c. Then the question arises whether there is a set of variables which advances the bifurcation with $\alpha_{th} < 0$ and thus de-stabilizes the system. Applying the definitions in Eq. (19) to the definition of α_{th} in (67), we find

$$\alpha_{th} = \frac{2\beta_c\beta_0}{\alpha_0^2} - 3\frac{\gamma_c}{|\alpha_0|} = \frac{2}{|\Omega|}\frac{\mathcal{F}[K_2](k_c)\mathcal{F}[K_2](k_0)}{\mathcal{F}[K_1]^2(k_0)} - \frac{3}{|\Omega|}\frac{\mathcal{F}[K_3](k_c)}{|\mathcal{F}[K_2](k_0)|}$$

and subsequently

$$\alpha_{th} = \frac{\eta^2}{2|\Omega|S_c'}\frac{1}{|S'[U_0](a_e - a_i) - 1|} \times \left(\frac{a_e - a_i}{|S'[U_0](a_e - a_i) - 1|}\left(S''[U_0]\right)^2 - S'''[U_0]\right). \quad (72)$$

Here we used the definition of the threshold

$$\alpha_c = \mathcal{F}[K_1](k_c) = S_c'(\mathcal{F}[K](k_c) + \mathcal{F}[L](k_c)) - 1 = 0.$$

with k_c taken from (14) and critical value S_c'. From Eq. (72) we learn that the bifurcation shift is independent of the spatial kernel but depends on the stationary state U_0 and the total excitatory and inhibitory synaptic weight a_e and a_i, respectively. Further, the prefactor in Eq. (72) is positive for $a_e > a_i$, and yet an advanced bifurcation with $\alpha_{th} < 0$ is possible for $S'''[U_0] > 0$ only. In the present application, the specific choice of the stationary state U_0 yields $\gamma_c < 0$, i.e. $S'''[U_0] < 0$, and thus $\alpha_{th} > 0$, i.e. a delayed bifurcation.

5.3. Spatially global fluctuations in the IDE

In addition, the stochastic full model (1) has been studied numerically. The time integration obeyed a stochastic Runge–Kutta algorithm of second order [71] with time step dt = 0.005 and random equally distributed initial values in the interval $[-0.025; 0.025]$. Further, the integration over space obeyed the trapezoidal rule with the spatial grid of 400 intervals

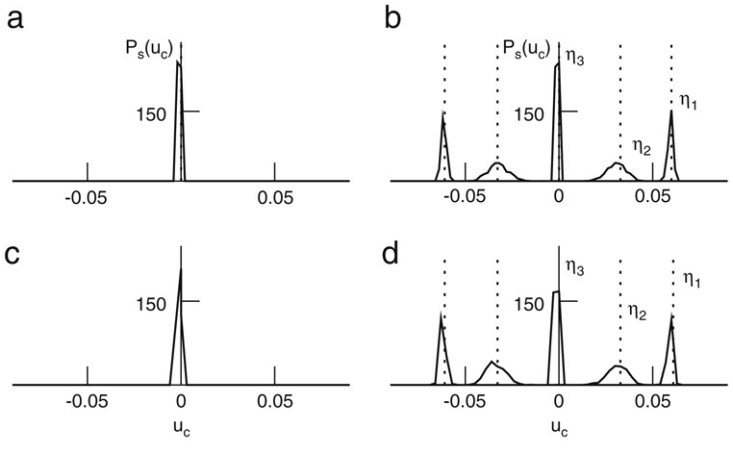

Fig. 8. The stationary probability density $P_s(u_c)$ computed for global fluctuations at order $O(\varepsilon^{5/2})$ at two different values of U_0, for different number of modes and different fluctuation strengths. The top row shows $P_s(u_c)$ for two spatial modes u_0 and u_c computed from Eqs. (64) and (65) (a) for $U_0 = 3.1$ for the fluctuation strength $\eta = 0.01$ and (b) $U_0 = 3.0$ for the fluctuation strengths $\eta_1 = 0.01$, $\eta_2 = 0.02$ and $\eta_3 = 0.03$. The bottom row shows $P_s(u_c)$ for three spatial modes u_0, u_c and u_{2c} computed from Eqs. (18) for (c) $U_0 = 3.1$ for $\eta_1 = 0.01$ and (d) $U_0 = 3.0$ for the same values of η_1, η_2, η_3 as in (b). The vertical dotted lines represent the stationary states obtained from the analytical studies in Section 4.6. Further parameters are taken from Figs. 2 and 4.

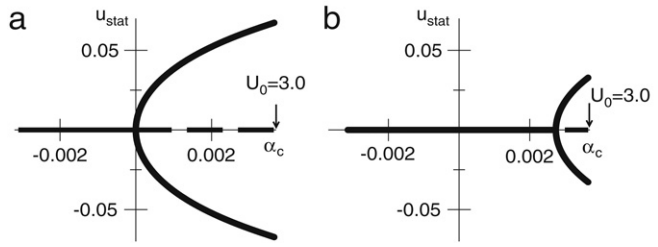

Fig. 9. The bifurcation diagram of the order parameter equation at orders $O(\varepsilon^{5/2})$ in the absence and the presence of global fluctuations corresponding to Eq. (68) with $u_{\text{stat}} = u_n$. In (a) $\eta = 0$ and (b) considers the fluctuation strengths $\eta_2 = 0.02$, cf. Fig. 8. Solid lines denote stable stationary states and dashed lines encode unstable stationary states. Further parameters are taken from Fig. 8.

and the field length $|\Omega|$. Fig. 10(a) shows the space–time activity in the absence and presence of global fluctuations. We observe the onset of a spatial pattern in the absence of random fluctuations (left panel), while global fluctuations stabilize the system and no spatial pattern occurs (right panel). A closer statistical examination of the spatial pattern at a single time point in the stationary regime confirms this finding (Fig. 10(b)). Here the Fourier amplitude u_n of the stationary pattern exhibits strong peaks at $k = 0$ and $k = k_c = 1.3$ in the case of $\eta' = 0$ (left panel), while the peak at $k = k_c$ vanishes for $\eta' = 0.03$ (right panel). Eventually Fig. 10(c) shows the probability density of the Fourier amplitude $P_s(u_c)$ at $k = k_c$ computed in a large time window in the stationary regime. We observe a sharp peak at large Fourier amplitudes for $\eta' = 0$, while $P_s(u_c)$ for $\eta' > 0$ peaks at $u_c \approx 0$.

5.4. Sum of global and uncorrelated fluctuations in the IDE

Finally, let us investigate the effect of global fluctuations in the presence of intrinsic thermal fluctuations. We wish to see whether the postponement effect we have found survives in the presence of such uncorrelated noise. Such fluctuations may represent the sum of several different random background processes in the neural system and thus are spectrally white in space and time according to the central limit theorem. Then the neural field equation reads

$$\mathrm{d}U(x,t) = \left(-U(x,t) + \int_\Omega \mathrm{d}y\,(K(x-y) + L(x-y)) \times S[U(y,t)]\right)\mathrm{d}t + \eta_b \mathrm{d}Y(x,t) + \eta' \mathrm{d}W(t) \quad (73)$$

with the fluctuation strength η_b of the background fluctuations described by the differentials of a Wiener process in space and time $\mathrm{d}Y(x,t)$ with $\langle \mathrm{d}Y(x,t)\rangle = 0$, $\langle \mathrm{d}Y(x,t)\mathrm{d}Y(y,\tau)\rangle = 2\delta(x-y)\delta(t-\tau)\mathrm{d}t\,\mathrm{d}\tau$.

Fig. 11(a) shows the spatio-temporal activity of the system in the presence of uncorrelated background fluctuations and the sum of background and global fluctuations. It turns out that the sum of both fluctuation types makes the spatial Turing pattern vanish (Fig. 11(a)). This is confirmed by the numerical computation of the spatial Fourier spectrum (Fig. 11(b)) and the probability density $P_s(u_c)$ (Fig. 11(c)) which reveal the lacking contribution of the critical spatial mode k_c in the presence of global fluctuations. Hence, global fluctuations delay the Turing bifurcation in the neural system even in the presence of background fluctuations.

6. Application to the Swift–Hohenberg equation

Now we apply the analytical and numerical analysis to the Swift–Hohenberg equation (SHE), which describes the amplitude dynamics in the Rayleigh–Benard convection near the onset of a stationary, i.e. time-independent, instability [69, 72]. As has been shown in [55], the SHE can be derived as

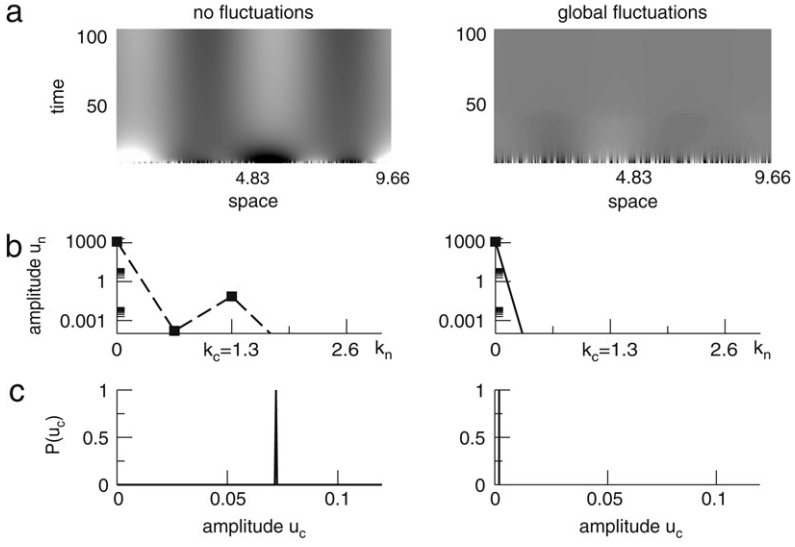

Fig. 10. Effects of global fluctuations on the full system (1). In (a), the spatio-temporal activity is shown subtracted from its spatial average at each time for the fluctuation strengths $\eta' = 0$ (left) and $\eta' = 0.03$ (right). (b) Absolute values of the spatial modes u_n at wavenumbers k_n at an arbitrary time point in the stationary regime of the system. (c) Stationary probability density $P(u_c)$ of the stationary amplitude values u_c at $k = k_c = 1.3$ in the time window $87 < t < 214$ (no fluctuations, left panel) and $231 < t < 331$ (global fluctuations, right panel) in the stationary regime of the system. Further parameters are taken from Fig. 8.

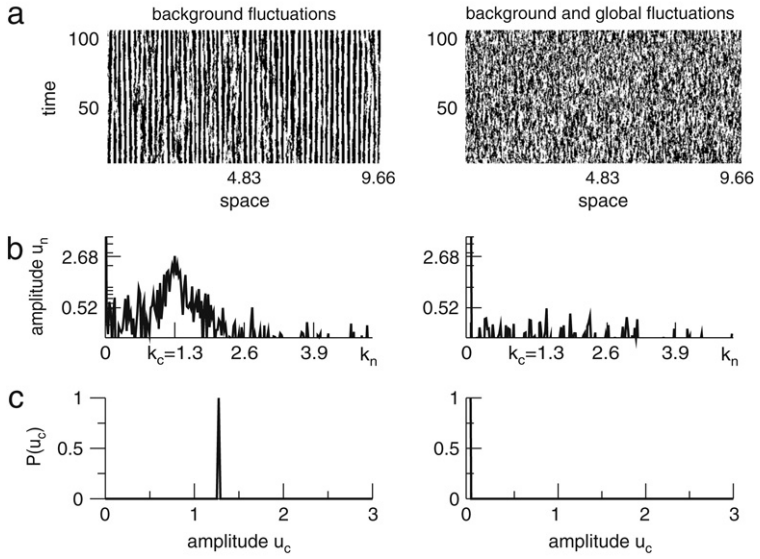

Fig. 11. Effects of global fluctuations on the full neural field equation (73) in the presence of background fluctuations. In (a), the spatio-temporal activity is shown subtracted from its spatial average at each time for background fluctuations with $\eta_b = 0.005$, $\eta' = 0$, and for the sum of background and global fluctuations with $\eta_b = 0.005$, $\eta' = 0.2$. (b) shows the absolute values of the spatial modes u_n at wavenumbers k_n at $t = 1076$ in the stationary regime of the system. In (c) the panels give the stationary probability density $P(u_c)$ of the stationary amplitude values u_c at $k = k_c = 1.3$ in the time window $1076 < t < 1176$ (left panel) and $182 < t < 282$ (right panel) in the stationary regime of the system.

a specific case of Eq. (1). To this end we specify $h[U] = aU - bU^3$, $b > 0$, $S_K[U] = -U$ and $S_L = 0$, and we obtain

$$\frac{\partial U(x,t)}{\partial t} = aU(x,t) - bU^3(x,t) - \int_\Omega K(x-y)U(y,t) + I(x,t). \tag{74}$$

Then the integral in Eq. (74) can be approximated by a sum of partial differentials with respect to $U(x,t)$, and we obtain

$$\frac{\partial U(x,t)}{\partial t} = aU(x,t) - bU^3(x,t) - K_0U(x,t) - K_2\frac{\partial^2}{\partial x^2}U(x,t) - K_4\frac{\partial^4}{\partial x^4}U(x,t) + I(x,t) \tag{75}$$

with the kernel moments $K_n = \int_\Omega \mathrm{d}z z^n K(z)/n!$. Specifically we choose the spatial kernel $K(x)$ as a Gaussian distribution $N(0,\sigma^2)$ with vanishing mean and a variance σ. In other words, σ represents the spatial interaction range of the system [55]. Then the choice $b = 1/2$ and the re-scaling of time and space according to $t \to 2t$ and $x \to \sigma x/\sqrt{2}$ yield the SHE

$$\frac{\partial U(x,t)}{\partial t} = \varepsilon U(x,t) - U^3(x,t) - \left(1 + \frac{\partial^2}{\partial x^2}\right)^2 U(x,t) + I(x,t) \tag{76}$$

with the control parameter $\varepsilon = 2a - 1$. In the following we assume periodic boundary conditions.

Following the analysis steps in Section 4, we have

$$\frac{\delta S_K}{\delta U} = -1, \quad \frac{\delta^2 S_K}{\delta U^2} = 0, \quad \frac{\delta^3 S_K}{\delta U^3} = 0$$

and

$$\alpha_n = \varepsilon - 1 + 2k_n^2 - k_n^4, \quad \beta_n = 0, \quad \gamma_n = \gamma = -\frac{1}{|\Omega|}.$$

In addition, the threshold shift is obtained from Eq. (67) to

$$\alpha_{th} = \frac{3\gamma}{|\alpha_0|}\eta^2 > 0,$$

i.e. the system is stabilized by the global fluctuations.

The stationary state U_0 constant in space and time is given by $U_0 = 0$ for all ε and $U_0 = \pm\sqrt{\varepsilon}$ for $\varepsilon > 0$. In the following we choose $U_0 = 0$, and the stochastic SHE is given by

$$\mathrm{d}U(x,t) = \left(\varepsilon U(x,t) - U^3(x,t) - \left(1 + \frac{\partial^2}{\partial x^2}\right)^2 U(x,t)\right)\mathrm{d}t + \mathrm{d}\Gamma(x,t)$$

with $\mathrm{d}\Gamma(x,t)$ taken from (5). Further, we specify the domain as a circle of circumference $|\Omega| = 80\pi$. This choice of $|\Omega| = 80\pi$ guarantees numerically the normalization of the kernel and the de-stabilization of a single spatial mode. This means that the discrete wavenumbers are given by $k_n = 0.025n$, $n \in \mathcal{Z}_0$. With this parameter choice $\varepsilon > 0$ yields a single unstable mode with $\alpha_c > 0$ at $|k_c| = 1$ and stable modes with $\alpha_n < 0$ for $|k_n| \neq 1$. For $\varepsilon < 0$, all modes are stable with $\alpha_n < 0$. Fig. 12 illustrates the dependence of α_n of the wavenumbers k_n. To compare the analytical results on global fluctuations with numerical results, we applied the stochastic Euler forward algorithm with $\mathrm{d}t = 0.01$ for the amplitudes $u_c(t)$, u_0 and u_{2c} at order $O(\varepsilon^{5/2})$. The initial values of the modes were taken from a uniform distribution in the interval $[-0.4; 0.4]$, and the stationary probability density $P_s(u_c)$ was computed by an ensemble average over 1000 simulated paths. The stationary state was reached after 4×10^5 time steps.

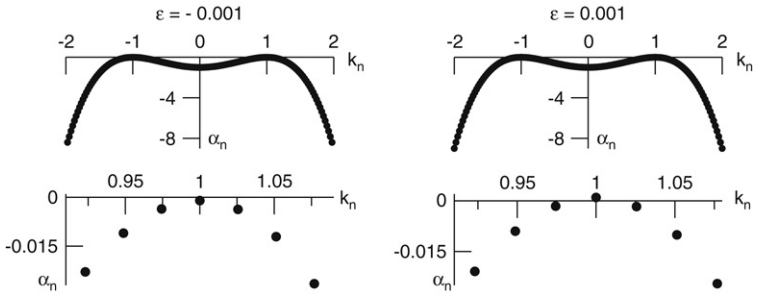

Fig. 12. The values of α_n subject to the wavenumber k_n for two values of the control parameter ε. The panels on the bottom represent the same data as in the top line but focussed on a smaller range of values.

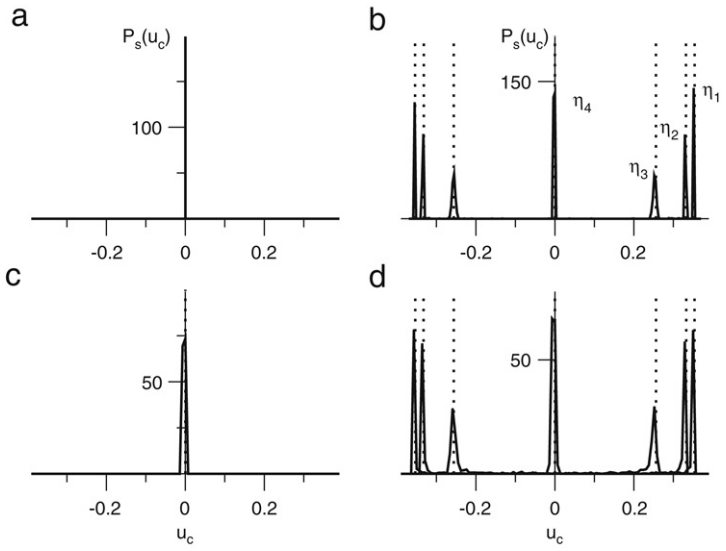

Fig. 13. The probability density $P_s(u_c)$ computed numerically at order $O(\varepsilon^{5/2})$ in the presence of global fluctuations for two and three modes and different fluctuation strengths. The top row shows results from the mode equations (64) and (65) of the modes u_c, u_0 at (a) $\varepsilon = -0.001$ for $\eta = 0.1$ and (b) $\varepsilon = 0.001$ for $\eta_1 = 0$, $\eta_2 = 0.1$, $\eta_3 = 0.2$, $\eta_4 = 0.4$. The bottom row shows numerical results for the modes u_c, u_0 and u_{2c} taken from (18) at (c) $\varepsilon = -0.001$ for $\eta = 0.1$ and (d) $\varepsilon = 0.001$ for the same fluctuation strengths as in (b). The vertical dotted lines denote the analytical solution (69).

The numerical results are shown in Fig. 13; see also [43]. At first it turns out that the results gained from the modes u_c, u_0 coincide with the results from three modes u_c, u_0 and u_{2c}, which thus validates the approximation of neglecting higher modes in Section 4.6. Further, the numerical results represent good approximations of the analytical results and thus confirm the noise-induced shift of the bifurcation threshold. The corresponding bifurcation diagram is presented in Fig. 14 for two values of η, and we observe the noise-induced shift to higher values. In other words, the numerical results confirm the stabilization of the system by global fluctuations for the Swift–Hohenberg equation [43].

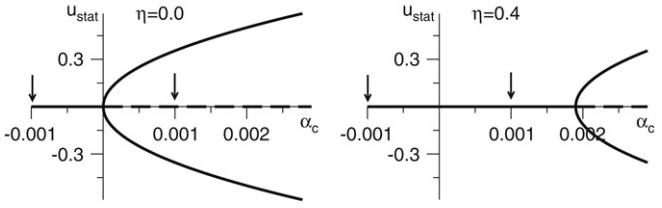

Fig. 14. Bifurcation diagram of the stationary amplitude u_{stat} taken from (68) subjected to the control parameter $\alpha_c = \varepsilon$ for two values of η. The vertical arrows denote the values of α_c examined in Fig. 13. Solid lines (dashed lines) denote stable (unstable) solutions.

7. Conclusion

Our work studies the impact of additive fluctuations on spatially extended systems analytically and numerically. The major element of the work is the combination of two stochastic perturbation methods, namely the stochastic center manifold approach for stochastic differential equations and the adiabatic elimination procedure for Fokker–Planck equations. Both latter methods allow for the analytical treatment of spatial systems near the bifurcation threshold. Further, the combination of both methods has been studied for two types of random fluctuation. We find that fluctuations uncorrelated in both time and space do not affect the stability of spatial systems. In contrast, global fluctuations, i.e. spatially constant fluctuations uncorrelated in time, do change the stability of the system near the bifurcation threshold. This effect is derived analytically and is confirmed quantitatively in numerical simulations. Specifically,

the bifurcation threshold of the system is shifted proportionally to the variance of the global fluctuations. To gain some insight into the bifurcation shift, the proposed approach is applied to a neural field equation and the Swift–Hohenberg equation. We observe a positive shift of the bifurcation threshold to higher values in both models. In other words, additive global fluctuations delay the Turing bifurcation in both models.

Future work may aim to study random fluctuations correlated in space and time in one-dimensional spatial systems. Further two-dimensional spatial systems may be investigated due to their importance in physics, biology and chemistry.

Acknowledgements

A. Hutt and A. Longtin acknowledge the financial supported by NSERC (Canada), and L. Schimansky-Geier has been supported by the Deutsche Forschungsgemeinschaft (grant Sfb-555) and VW-foundation (3140 1201).

Appendix. Definition of variables

The following abbreviations have been used in Sections 4.5 and 4.6:

$$A = 16\frac{\beta_0}{\alpha_0^2}\left(2\frac{\beta_0 b}{\alpha_0} - \frac{\beta_0^2}{\alpha_0} + \gamma_0 - \gamma_c\right),$$

$$B = 4b\left(\gamma_0 + \frac{2\beta_0(b+\beta_0)}{\alpha_0}\right)$$

$$C = a - 8\frac{\beta_0 b\alpha_c}{\alpha_0^2}, \quad D = A + 48\frac{\gamma_c\beta_0^2}{\alpha_0^2}.$$

References

[1] M. Walgraef, Spatio-Temporal Pattern Formation, Springer, New York, 1996.
[2] J.D. Murray, Mathematical Biology, Springer, Berlin, 1989.
[3] P. Nunez, Neocortical Dynamics and Human EEG Rhythms, Oxford University Press, New York, Oxford, 1995.
[4] G.B. Ermentrout, J.D. Cowan, A mathematical theory of visual hallucination patterns, Biol. Cybern. 34 (1979) 137–150.
[5] P.C. Bressloff, J.D. Cowan, M. Golubitsky, P.J. Thomas, M.C. Wiener, What geometric visual hallucinations tell us about the visual cortex, Neural Comput. 14 (2002) 473–491.
[6] F. Wolf, Symmetry, multistability, and long-range interactions in brain development, Phys. Rev. Lett. 95 (2005) 208701.
[7] S. Coombes, Waves, bumps and patterns in neural field theories, Biol. Cybern. 93 (2005) 91–108.
[8] V.K. Jirsa, Connectivity and dynamics of neural information processing, Neuroinformatics 2 (2) (2004) 183–204.
[9] V.K. Jirsa, K.J. Jantzen, A. Fuchs, J.A.S. Kelso, Spatiotemporal forward solution of the EEG and MEG using network modelling, IEEE Trans. Med. Imag. 21 (5) (2002) 493–504.
[10] T. Wennekers, Orientation tuning properties of simple cells in area V1 derived from an approximate analysis of nonlinear neural field models, Neural Comput. 13 (2001) 1721–1747.
[11] D. Somers, S. Nelson, M. Sur, An emergent model of orientation selectivity in cat visual cortical simple cells, J. Neurosci. 15 (8) (1995) 5448–5465.
[12] R. Ben-Yishai, R. Bar-Or, H. Sompolinsky, Theory of orientation tuning in visual cortex, Proc. Natl. Acad. Sci. 92 (1995) 3844–3848.
[13] H. Haken, Synergetics, Springer, Berlin, 2004.
[14] G. Nicolis, I. Prigogine, Self-Organization in Non-Equilibrium Systems: From Dissipative Structures to Order Through Fluctuations, J. Wiley and Sons, New York, 1977.
[15] C. Gardiner, Handbook of Stochastic Methods, Springer, Berlin, 2004.
[16] W. Horsthemke, R. Lefever, Noise-induced Transitions, Springer, Berlin, 1984.
[17] B. Lindner, J. Garcia-Ojalvo, A. Neiman, L. Schimansky-Geier, Effects of noise in excitable systems, Phys. Rep. 392 (2004) 321–424.
[18] J. Garca-Ojalvo, J.M. Sancho, Noise in Spatially Extended Systems, Springer, New York, 1999.
[19] F. Sagus, J.M. Sancho, J. Garcia-Ojalvo, Spatiotemporal order out of noise, Rev. Modern Phys. 79 (2007) 829–882.
[20] H. Malchow, W. Ebeling, R. Feistel, L. Schimansky-Geier, Stochastic bifurcations in a bistable reaction–diffusion system with Neumann boundary conditions, Ann. Physik 40 (1983) 151.
[21] L. Schimansky-Geier, A.V. Tolstopjatenko, W. Ebeling, Noise-induced transitions due to external additive noise, Phys. Lett. A 108 (7) (1985) 329–332.
[22] E. Knobloch, K. Wiesenfeld, Bifurcations in fluctuating systems: The center-manifold approach, J. Stat. Phys. 33 (3) (1983) 611–637.
[23] C. van den Broeck, M. Malek Mansour, F. Baras, Asymptotic properties of coupled non-linear Langevin equations in the limit of weak noise, I: Cusp bifurcation, J. Stat. Phys. 28 (1982) 557.
[24] N. Berglunda, B. Gentz, Geometric singular perturbation theory for stochastic differential equations, J. Differential Equations 191 (2003) 1–54.
[25] G. Schoener, H. Haken, The slaving principle for Stratonovich stochastic differential equations, Z. Phys. B 63 (1986) 493–504.
[26] O. Carrillo, M.A. Santos, J. Garca-Ojalvo, J.M. Sancho, Spatial coherence resonance near pattern-forming instabilities, Europhys. Lett. 65 (2004) 452.
[27] J. Garca-Ojalvo, J.M. Sancho, External fluctuations in a pattern-forming instability, Phys. Rev. E 53 (6) (1996) 5680–5689.
[28] J. Garca-Ojalvo, A. Hernandez-Machado, J.M. Sancho, Effects of external noise on the Swift–Hohenberg equation, Phys. Rev. Lett. 71 (10) (1993) 1542–1545.
[29] D. Bloemker, M. Hairer, G.A. Pavliotis, Modulation equations: Stochastic bifurcation in large domains, Commun. Math. Phys. 258 (2005) 479–512.
[30] R. Kawai, X. Sailer, L. Schimansky-Geier, C. Van den Broeck, Macroscopic limit cycle via pure noise-induced phase transition, Phys. Rev. E 69 (3) (2004) 051104.
[31] T.D. Frank, Maier-Saupe model of liquid crystals: Isotropic-nematic phase transitions and second-order statistics studied by Shiino's perturbation theory and strongly nonlinear Smoluchowski equations, Phys. Rev. E 72 (4) (2005) 041703.
[32] D. Valenti, L. Schimansky-Geier, X. Sailer, B. Spagnolo, Moment equations for a spatially extended system of two competing species, Eur. Phys. J. B 50 (2006) 199–203.
[33] A. Hutt, T.D. Frank, Critical fluctuations and 1/f -activity of neural fields involving transmission delays, Acta Phys. Pol. A 108 (6) (2005) 1021.
[34] T. Frank, A. Daffertshofer, P. Beek, H. Haken, Impacts of noise on a field theoretical model of the human brain, Physica D 127 (1999) 233–249.
[35] T. Frank, A. Daffertshofer, C. Peper, P. Beek, H. Haken, Towards a comprehensive theory in brain activity: Coupled oscillator systems under external forces, Physica D 144 (2000) 62–86.
[36] X. Sailer, D. Hennig, V. Beato, H. Engel, L. Schimansky-Geier, Regular patterns in dichotomically driven activator-inhibitor dynamics, Phys. Rev. E 73 (2006) 056209.
[37] H. Risken, The Fokker–Planck equation—Methods of Solution and Applications, Springer, Berlin, 1989.
[38] F. Drolet, J. Vinals, Adiabatic elimination and reduced probability distribution functions in spatially extended systems with a fluctuating control parameter, Phys. Rev. E 64 (2001) 026120.
[39] M.A. Zaks, X. Sailer, L. Schimansky-Geier, A.B. Neiman, Noise induced complexity: From subthreshold oscillations to spiking in coupled excitable systems, Chaos 15 (2) (2005) 026117.

[40] C. Xu, A. Roberts, On the low-dimensional modelling of Stratonovich stochastic differential equations, Physica A 225 (1996) 62–80.
[41] P. Boxler, A stochastic version of the center manifold theorem, Probab. Theory Related Fields 83 (1989) 509–545.
[42] F. Drolet, J. Vinals, Adiabatic reduction near a bifurcation in stochastically modulated systems, Phys. Rev. E 57 (5) (1998) 5036–5043.
[43] A. Hutt, A. Longtin, L. Schimansky-Geier, Additive global noise delays Turing bifurcations, Phys. Rev. Lett. 98 (2007) 230601.
[44] M. Wu, G. Ahlers, D.S. Cannell, Thermally induced fluctuations below the onset of Rayleigh-Bnard convection, Phys. Rev. Lett. 75 (1995) 1743–1746.
[45] S. Jabbari-Farouji, D. Mizuno, M. Atakhorrami, F.C. MacKintosh, C.F. Schmidt, E. Eiser, G.H. Wegdam, D. Bonn, Fluctuation-dissipation theorem in an aging colloidal glass, Phys. Rev. Lett. 98 (2007) 108302.
[46] J. Garca-Ojalvo, J.M. Sancho, Colored noise in spatially extended systems, Phys. Rev. E 549 (4) (1994) 2769–2778.
[47] A.W. Ghosh, S.V. Khare, Rotation in an asymmetric multidimensional periodic potential due to colored noise, Phys. Rev. Lett. 84 (23) (2000) 5243–5246.
[48] P. Lam, D. Bagayoko, Spatiotemporal correlation of colored noise, Phys. Rev. E 48 (5) (1993) 3267–3270.
[49] H. Wang, K. Zhang, Q. Ouyng, Resonant-pattern formation induced by additive noise in periodically forced reaction–diffusion systems, Phys. Rev. E 74 (2006) 036210.
[50] A.K. Horvath, M. Dolnik, A.P. Munuzuri, A.M. Zhabotinsky, I.R. Epstein, Control of Turing structures by periodic illumination, Phys. Rev. Lett. 83 (15) (1999) 2950–2952.
[51] A. Sanz-Anchelergues, A.M. Zhabotinsky, I.R. Epstein, A.P. Munuzuri, Turing pattern formation induced by spatially correlated noise, Phys. Rev. E 63 (2001) 056124.
[52] Th. John, R. Stannarius, U. Behn, On-off intermittency in stochastically driven electrohydrodynamic convection in nematics, Phys. Rev. Lett. 83 (4) (1999) 749–752.
[53] A. Hutt, M. Bestehorn, T. Wennekers, Pattern formation in intracortical neuronal fields, Network: Comput. Neural Syst. 14 (2003) 351–368.
[54] A. Hutt, F.M. Atay, Analysis of nonlocal neural fields for both general and gamma-distributed connectivities, Physica D 203 (2005) 30–54.
[55] A. Hutt, Generalization of the reaction–diffusion, Swift–Hohenberg, and Kuramoto–Sivashinsky equations and effects of finite propagation speeds, Phys. Rev. E 75 (2007) 026214.
[56] G.B. Ermentrout, Neural networks as spatio-temporal pattern-forming systems, Rep. Progr. Phys. 61 (1998) 353–430.
[57] R. Curtu, Ermentrout, Pattern formation in a network of excitatory and inhibitory cells with adaption, SIAM J. Appl. Dyn. Syst. 3 (3) (2004) 191–231.
[58] C. Laing, W. Troy, PDE methods for non-local models, SIAM J. Appl. Dyn. Syst. 2 (3) (2003) 487–516.
[59] A.A. Zaikin, J. Garca-Ojalvo, L. Schimansky-Geier, Nonequilibrium first-order phase transition induced by additive noise, Phys. Rev. E 60 (6) (1999) R6275–R6278.
[60] D. Bloemker, Amplitude equations for locally cubic non-autonomous nonlinearities, SIAM J. Appl. Dyn. Syst. 2 (2) (2003) 464–486.
[61] B. Doiron, M. Chacron, L. Mahler, A. Longtin, J. Bastian, Inhibitory feedback required for network burst responses to communication but not to prey stimuli, Nature 421 (2003) 539–543.
[62] F.M. Atay, A. Hutt, Stability and bifurcations in neural fields with finite propagation speed and general connectivity, SIAM J. Appl. Math. 65 (2) (2005) 644–666.
[63] A. Turing, The chemical basis of morphogenesis, Philos. Trans. R. Soc. London 327B (1952) 37–72.
[64] V. Castets, E. Dulos, J. Boissonade, P.D. Kepper, Experimental-evidence of a sustained standing Turing-type non-equilibrium chemical-pattern, Phys. Rev. Lett. 64 (1990) 2953–2956.
[65] L. Perko, Differential Equations and Dynamical Systems, Springer, Berlin, 1998.
[66] P. Jung, A. Neiman, M. Afghan, S. Nadkarni, G. Ullah, Thermal activation by power-limited coloured noise, New J. Phys. 7 (2005) 17.
[67] P. Haenggi, P. Jung, Colored noise in dynamical systems, Adv. Chem. Phys. 89 (1995) 239–326.
[68] M. Carandini, D. Ringach, Predictions of a recurrent model of orientation selectivity, Vision Res. 37 (21) (1997) 3061–3071.
[69] M.C. Cross, P.C. Hohenberg, Pattern formation outside of equilibrium, Rev. Modern Phys. 65 (3) (1993) 851–1114.
[70] N.A. Venkov, S. Coombes, P.C. Matthews, Dynamic instabilities in scalar neural field equations with space-dependent delays, Physica D 232 (2007) 1–15.
[71] R.L. Honeycutt, Stochastic Runge–Kutta algorithms, I. white noise, Phys. Rev. A 45 (2) (1992) 600–603.
[72] J.B. Swift, P.C. Hohenberg, Hydrodynamic fluctuations at the convective instability, Phys. Rev. A 15 (1977) 319.